This is the Pre-Published Version.
This is the peer reviewed version of the following article: Chen, Zijian; Lu, Xi; Wang, Huixin; Chang, Jian; Wang, Dongrui; Wang, Wenshuo; Ng, Sze-Wing; Rong, Mingming; Li, Peng; Huang, Qiyao; Gan, Zhuofei; Zhong, Jianwen; Li, Wen-Di; Zheng, Zijian(2023). Electrochemical Replication and Transfer for Low-Cost, Sub-100 nm Patterning of Materials on Flexible Substrates. Advanced Materials, 35(10), 2210778, which has been published in final form at https://doi.org/10.1002/adma.202210778.

Electrochemical replication and transfer for low-cost, sub-100 nm patterning of materials on flexible substrates

*Zijian Chen†, Xi Lu†, Huixin Wang, Jian Chang, Dongrui Wang, Wenshuo Wang, Sze-Wing Ng, Mingming Rong, Peng Li, Qiyao Huang, Zhuofei Gan, Jianwen Zhong, Wen-Di Li, Zijian Zheng**

†These authors contributed equally to this work.

Zijian Chen, Xi Lu, Huixin Wang, Jian Chang, Dongrui Wang, Wenshuo Wang, Sze-Wing Ng, Mingming Rong, Peng Li, Qiyao Huang, Zijian Zheng
School of Fashion and Textiles, The Hong Kong Polytechnic University, Hong Kong SAR, China.
E-mail: tczzheng@polyu.edu.hk

Zhuofei Gan, Jianwen Zhong, Wen-Di Li
Department of Mechanical Engineering, The University of Hong Kong, Hong Kong SAR, China.

Zijian Zheng
Department of Applied Biology and Chemical Technology, The Hong Kong Polytechnic University, Hong Kong SAR, China.
State Key Laboratory for Ultra-precision Machining Technology, The Hong Kong Polytechnic University, Hong Kong SAR, China.
Research Institute for Intelligent Wearable Systems, The Hong Kong Polytechnic University, Hong Kong SAR, China.
Research Institute for Smart Energy, The Hong Kong Polytechnic University, Hong Kong SAR, China.

This article may be used for non-commercial purposes in accordance with Wiley Terms and Conditions for Use of Self-Archived Versions. This article may not be enhanced, enriched or otherwise transformed into a derivative work, without express permission from Wiley or by statutory rights under applicable legislation. Copyright notices must not be removed, obscured or modified. The article must be linked to Wiley's version of record on Wiley Online Library and any embedding, framing or otherwise making available the article or pages thereof by third parties from platforms, services and websites other than Wiley Online Library must be prohibited.

Keywords: nanofabrication, flexible electronics, additive manufacture, electrochemistry, pattern transfer

The fabrication of high-resolution patterns on flexible substrates is an essential step in the development of flexible electronics, However, the patterning process on flexible substrates often requires expensive equipment and tedious lithographic processing. We report here a bottom-up patterning technique, termed electrochemical replication and transfer (ERT), which fabricates multi-scale patterns of a wide variety of materials by selective electrodeposition of target materials on a pre-defined template, and subsequent transfer of the electrodeposited materials to a flexible substrate, while leaving the undamaged template for reuse for over 100 times. The additive and parallel patterning attribute of ERT allows the fabrication of multi-scale patterns with resolutions spanning from sub-100 nm to many cm simultaneously, which overcomes the tradeoff between resolution and throughput of conventional patterning techniques. ERT is suitable for fabricating a wide variety of materials including metals, semiconductors, metal oxides, and polymers into arbitrary shapes on flexible substrates at a very low cost.

1. Introduction

Patterning materials on flexible substrates at multiple length scales spanning from sub-100 nanometer to many micrometers is a fundamental step to fabricate electronic, photonic, biological and medical devices for different flexible and wearable applications [1]. Unlike the ultra-smooth and easy-to-clean rigid substrates used in the traditional photonic and electronic industries, flexible substrates are often much rougher, difficult to wet, incompatible with strong solvents, and unstable to thermal annealing, which have led to significant challenges in the patterning process [2].

Nowadays, the most reported patterning strategy on flexible substrates is to firstly fabricate the desirable patterns on rigid substrates (such as Si) through conventional lithographic techniques such as photolithography [3], electron-beam lithography (EBL)

[4], and nanoimprint lithography (NIL) [5], followed by transfer of the patterns onto targeted flexible substrates [6]. This strategy disassociates the lithographic steps from the flexible substrate, so that it can realize complex structures with a high resolution predominately defined by the lithographic method used [7]. However, because the lithographic process is involved in every fabrication, this strategy requires tedious procedures and is very costly [8]. The throughput is limited in the range of 10^{-6} to 1 m^2/h [9].

In contrast, printing techniques such as inkjet printing, screen printing, flexo and gravure printings, and contact printing are low-cost and user-friendly to fabricate patterns directly on flexible substrates [10]. The compatibility of printing techniques with roll-to-roll process significantly improves the throughput to an ultrahigh level of as much as 10^3 m^2/h [11]. However, the patterning resolution of printing is typically in the order of several to tens of micrometers, which cannot satisfy the needs for making micro- and nano-devices [12].

Soft lithography represented by microcontact printing and its derivatives has been developed in the decades [13]. Soft lithography makes use of a soft stamp to transfer molecules and materials from a pre-made template to a target substrate by means of printing and molding. The soft lithography was originally developed to address cost-effective and throughput issues of conventional lithography. Indeed, there are numerous demonstrations that soft lithography can fabricate nanoscale structures [14]. Nevertheless, it is still very challenging to fabricate sub-100 nm features over a large area with soft lithography due to various reasons such as the softness of stamp, the diffusion of ink, the capillary pressure of nanofluidic, and the difficulty to control the contact uniformity over a large distance [15].

Indeed, there is still a lack of cost-effective technique for high-throughput and high-resolution patterning of a wide variety of materials on flexible substrates to date. In this paper, we report a new patterning technique named electrochemical replication and transfer (ERT), which combines the advantages of both lithography and printing strategies to address the tradeoff among the three most important patterning parameters,

being resolution, throughput and cost. ERT fabricates patterns on flexible substrates in ambient environment via two simple steps: 1) electrochemical deposition of patterned materials on a pre-made Au template, and 2) transfer of the patterned materials from the Au template to the flexible substrate with a photo-curable binder, while the Au template is reused for the next patterning process. On one hand, the electrochemical replication mechanism allows to duplicate arbitrary patterns with different feature sizes spanning from sub-100 nm to cm on a large area within minutes. The pattern resolution is only limited to the pre-made template and the throughput of ERT can reach 10-10^2 m^2/h regardless of the feature size. On the other hand, the entire process is lithography-free and purely additive. The use of electrochemical deposition equipment ensures the ultra-low cost of the patterning process. ERT could fabricate thick high-quality pattern with various materials ranging from metals, metal oxide, semiconducting metal sulfide and polymers, which is superior to most soft lithography methods. The patterns can be readily made on a wide variety of flexible substrates including plastics, papers and textiles.

2. Fabrication process of ERT

The detailed fabrication process of ERT is schematically illustrated in **Figure 1A**. The reusable template was pre-made with traditional lithography routes such as photolithography and EBL. As a proof of concept, we demonstrated the ERT process using a 4-inch Au-patterned (25 nm thick Au with a 5 nm of Cr as the adhesive layer) Si template, which was comprised of multiple patterns of different shapes and sizes (Figure 1B and Movie 1). A self-assembled monolayer (SAM) of 1H,1H,2H,2H-perfluorodecanethiol (PFDT) was grown on the surface of Au, which served as the anti-adhesive release layer to facilitate the transfer of materials after the electrodeposition step and to improve the reusability of the Au template. The SAM-modified Au template was immersed in the specific electrodeposition solution to execute the electrochemical replication, i.e., the target material (such as Cu in Figure 1C) was site-selectively electrodeposited on the region of Au pattern under the optimized current density.

Subsequently, the as-deposited patterned material was transferred from the Au template onto the target flexible substrate (poly(ethylene terephthalate), PET) with the assistance of a photo-curable binder (Norland Optical Adhesive 63, NOA 63), shown in the top part in Figure 1D, leaving the Au-patterned template for reuse in the following many ERT processes (bottom in Figure 1D). In detail, NOA 63 binder was firstly cast onto the electrodeposited patterns. The targeting substrate, such as cloth, paper, and PET film, was then directly placed and pressed on the NOA-cast substrate. Upon the exposure to UV light, the binder layer was cured, which strongly adhered to both the electrodeposited patterns and the targeting substrate (i.e., cloth, paper, PET, etc.). By a simple peeling process, the electroplated pattern deposited on the Au template was transferred to the targeting substrate together with the binder. As a new patterning technique, ERT creates patterns within only two facile steps in the ambient environment, which is superior to those conventional lithography requiring multiple and tedious steps (Figure S1).

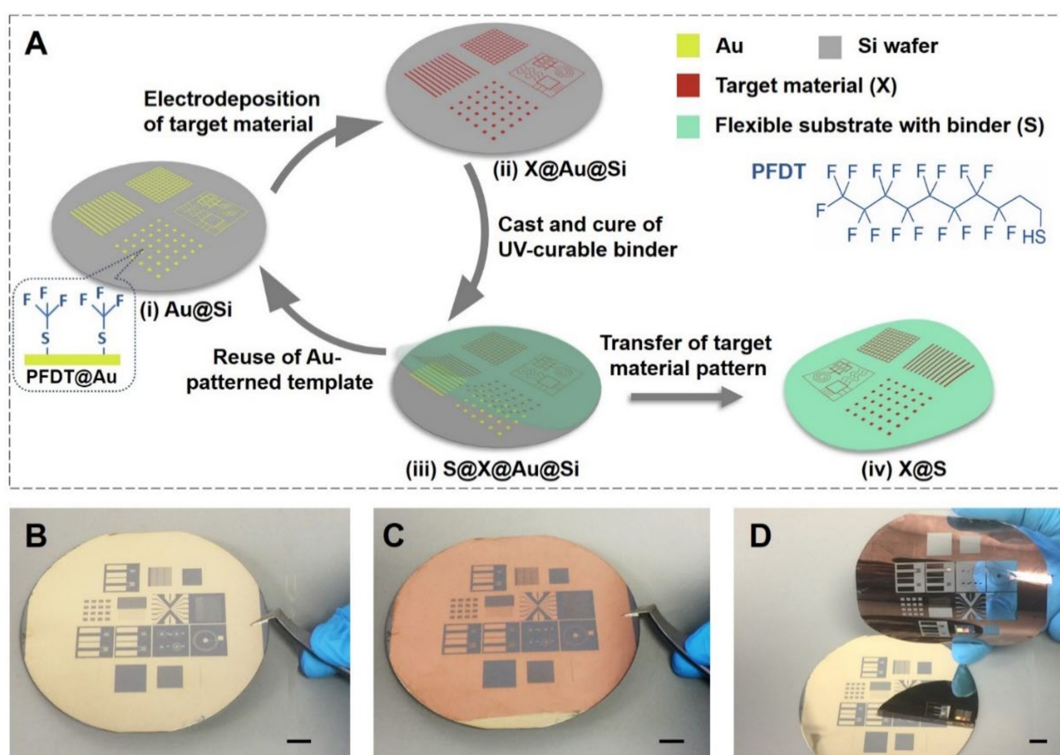

Figure 1. Fabrication process of electrochemical replication and transfer (ERT). (**A**) Schematic diagram of ERT method. (**B-D**) Wafer-scale demonstration of copper (Cu) patterns fabricated by ERT process. (**B**) Thin gold (Au) patterns on silicon (Si) wafer used as reusable template in ERT process. (**C**) Cu patterns obtained through electrochemical replication step, where Cu site-selectively electrodeposited on Au-patterned regions. (**D**) Cu patterns transferred into the target flexible substrate (PET/NOA 63) (top), and the Au-patterned template reused for the next fabrication cycle (bottom). Scale bars, 1 cm.

Figure 2A-F show the as-fabricated 4"-size Cu patterns on PET, which consists of four major categories of structures that are frequently used in device fabrication. Figure 2B represents feature arrays with a gradient change of feature size (in this case, linewidth) ranging from 500 nm to 10 μm. The second category is separated island-type features shown in Figure 2C and 2D, while the third one is interconnected meshes shown in Figure 2E and 2F. Figure 2G and 2H show the ability to fabricate both positive and negative patterns with the smallest feature sizes of ~2 μm. Figure 2I shows a complicated pattern of an integrated circuit, which consists of a combination of straight lines, serpentines, squares, circles, interdigital electrodes, etc. Thanks to the advantage of parallel replication, ERT process can fabricate all these patterns with different shapes and feature sizes on one substrate simultaneously. Importantly, unlike conventional protruded structures fabricated on the flexible substrate, the transferred patterns were embedded in the binder layer of the plastic substrate. Therefore, the surface roughness was as low as a few nm (Figure S2).

3. Microfabrication of Different Materials via ERT

Importantly, ERT is versatile to structure a wide variety of materials that, in principle, can be synthesized by electrochemical deposition such as electroplating and electropolymerization. As a proof of concept, we herein demonstrate the ERT method applicable to four major types of materials, including metals (Cu, Au, Ni, and Zn), metal

oxide (MnO_2), semiconducting metal sulfide (CdS), and polymers (PPy, PANi). These materials were successfully fabricated on PET via ERT, as shown in Figure 2J and Figure S3. It is also possible to adopt ERT to fabricate patterns with different materials on one substrate. We successfully demonstrated an interdigital electrode pattern with multi-materials. Such a pattern was achieved by respectively electroplating Ag and Cu on the opposite electrodes, followed by transferring to the flexible thin-film substrate (Figure S4). The deposition conditions are listed in Table S1, and the corresponding characterizations of these materials, including XRD, FTIR and Raman spectrum, are provided in Figure S5. Furthermore, apart from PET, patterns can also be transferred onto other flexible substrates, such as paper, cotton and nylon clothes (Figure S6) that are commonly used in flexible and wearable applications.

The category of target substrates could also be expanded by replacing NOA 63 with other binders, such as polyvinyl alcohol (PVA). As shown in Figure S7, a viscose aqueous solution of PVA was poured onto the electrodeposited patterns. After drying, the PVA formed a film itself, in which the electrodeposited patterns were embedded in the PVA film with a strong adhesion. We then peeled off the PVA film together with the embedded electrodeposited patterns from the template, and then placed onto the target substrate. Due to the strong hydrophilicity and the softness of the PVA film, the conformal adhesion to the targeted substrate was easily achieved. We then dissolved the PVA with water, leaving only the electrodeposited patterns transferred on the target substrate. In comparison to the use of NOA 63, the dissolvability of PVA enables a universal transfer process that is more compatible with different types of target substrates. Figure S8 shows several examples including rigid surfaces (e.g., glass sheet) and curved surfaces (e.g., glass bottle), as well as stretchable substrates (Ecoflex film). These are substrates that are difficult to be achieved with NOA 63.

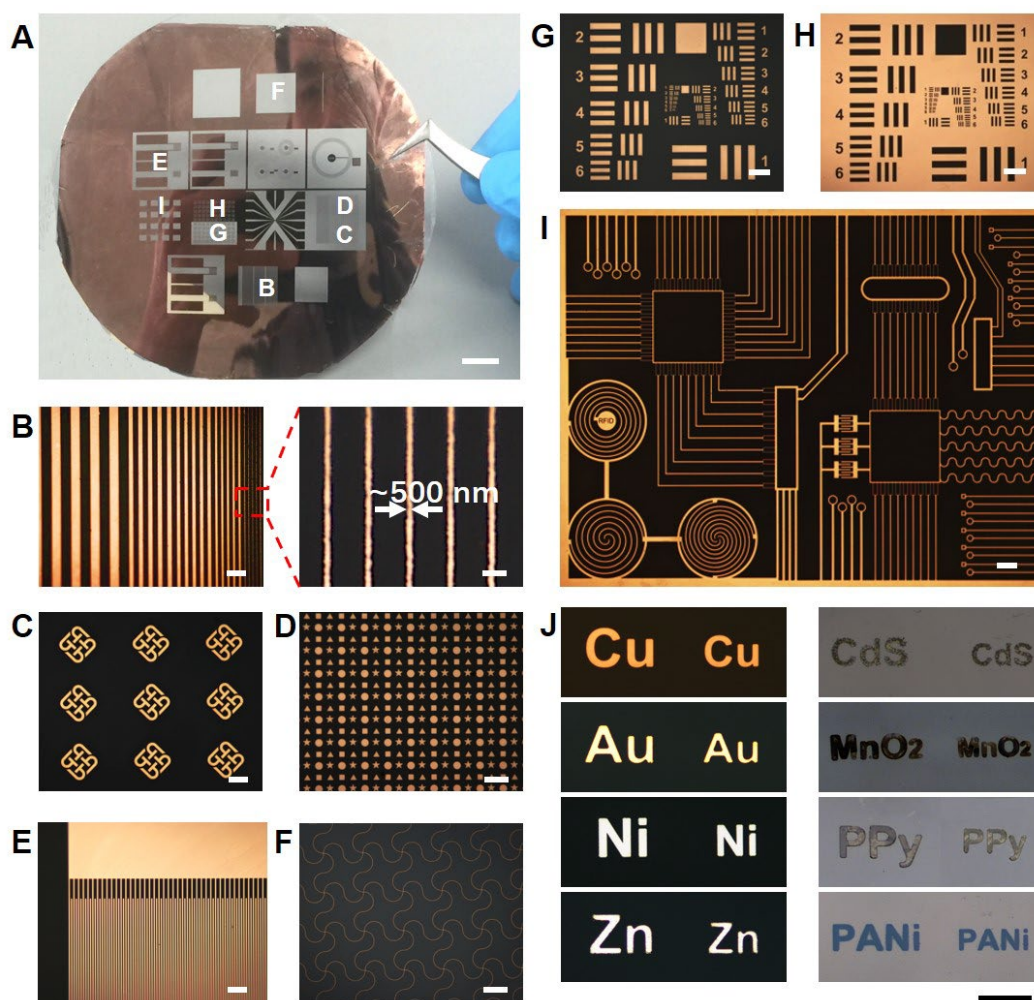

Figure 2. The applicability of ERT method to a wide range of geometric patterns and target materials. (**A**) A 4-inch wafer-scale Cu pattern fabricated by ERT method, the representative patterns marked as **B**-**I** on this wafer-scale sample and their details shown below. Scale bar, 1 cm. (**B**) Parallel stripes with linewidths spanning from 10 μm to ~500 nm. Scale bars, 20 μm (left); 2 μm (right). (**C, D**) Separated island-type pattern (**C**: the logo of The Hong Kong Polytechnic University; **D**: dots with different shapes). Scale bars, 100 μm. (**E, F**) Interconnected meshes. Scale bars, 100 μm. (**G, H**) A pair of positive and negative patterns with minimum feature sizes of ~2 μm. Scale bars, 100 μm. (**I**) An interconnection circuit pattern. The minimum linewidth, ~700 nm. Scale bars, 100 μm. (**J**) ERT method is applicable to a wide variety of materials: metals

(Cu, Au, Ni, and Zn), metal oxide (MnO_2), metal sulfide (CdS, semiconductor material), and polymers (PPy, PANi). Scale bar, 100 μm.

The surface modification of the Au patterns with PFDT is of critical importance to ensure the completion of pattern transfer and the reusability of the template in the ERT process (Figure 3). PFDT molecules formed a low-surface-energy self-assembled monolayer (SAM) on the Au surface (Figure 3A) [16], and it serves as an anti-adhesive layer which reduces the adhesion between the deposited materials and the Au surface. As an example, we fabricated Cu meshes via ERT. Without PFDT, a majority of areas of the Cu meshes were broken after the pattern transfer (Figure 3B). The template was also damaged significantly (Figure 3C). In contrast, the interfacial adhesion between Cu and Au reduced from 4 N to 0.2 N after modification with PFDT (Figure 3D), and the entire Cu mesh was transferred successfully from the Au template onto PET (Figure 3E). The template did not show any sign of damage and could be reused for more than 100 ERT fabrication cycles (Figure 3F and 3G). Based on a simple count of the whole template under the observation of optical microscopy, we did not find any defect on the Au pattern. Therefore, the defect density is nearly zero after 100 copies. Figure 3H displays the 100 replicas of Cu meshes on PET using the same template.

It should be noted that to ensure the large-area fabrication capability of ERT, the entire template is designed to be electrically conductive so that current can pass through for electrochemical deposition. The Si wafer is electrically conductive, even though its conductivity is 5~7 orders of magnitude lower than that of Au. In the ERT process, the electric current needs to pass through the entire template to the Au patterned areas. For those Au patterns that are interconnected, we may apply the current directly on the Au surface. However, for those discrete Au structures, the current will go through the Si wafer and then reach the Au patterns. When the feature size is in the micrometer scale, electrodeposition of target materials will preferentially occur on top of the Au region, because the electrical conductivity of Au is 5~7 orders of magnitude higher than that of Si (Tables S2-S3). Nevertheless, when the feature size decreased to sub-500 nm, we

noticed that the selectivity of electrodeposition became less controllable; random deposition of materials on Si surface often occurred (Figure S9).

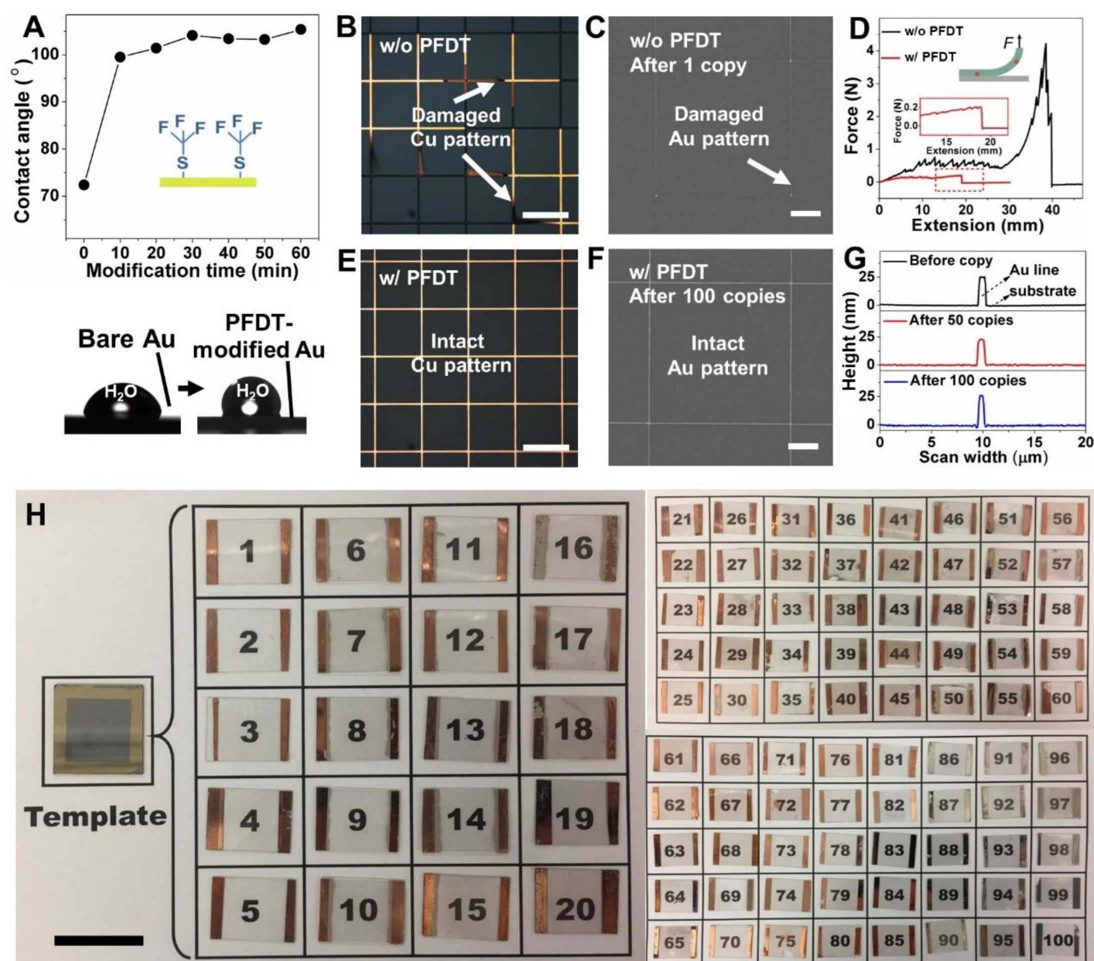

Figure 3. Functions of surface modification of self-assembled monolayer for ERT process. (**A**) Contact angles of Au film surface after modified by PFDT for different modification times. (**B**) Without PFDT modification, Cu pattern damaged seriously during the transfer process. Scale bar: 100 μm. (**C**) Without PFDT protection, Au pattern on template damaged during the mechanical peeling off process. Scale bar: 20 μm. (**D**) The forces of peeling off as-deposited Cu patterns from the Au-patterned templates with and without the pre-modification of PFDT. (**E**) With PFDT modification on Au-patterned template, as-deposited Cu pattern remained intact during transfer process. Scale bar: 100 μm. (**F**) With PFDT modification, Au pattern on template remained intact after 100 copies. Scale bar: 20 μm. (**G**) AFM characterization of the

profiles of Au lines on the same template before and after reuses (50 and 100 copies). (**H**) 100 Cu-mesh transparent electrodes fabricated by a single Au-patterned template. Size of transparent mesh, 1.5×1.5 cm^2. Scale bar, 1 cm.

4. Nanofabrication of ERT with Embedded Mold

To address the selectivity issue of nanopatterns, we made a simple improvement to the template by adding a thin layer of insulating silicon dioxide (SiO_2) around the Au patterns on Si, as shown in Figure 4A. The thickness of the SiO_2 was intentionally designed to be the same as that of the Au/Cr patterns so that all the Au structures will be embedded. As such, electrodeposition only occurred the conductive Au surface. This embedded structure could also reduce the contact area, and hence the contact adhesion between the Au pattern and the deposited materials. This was also significant to ease the pattern transfer of nanostructures and to protect the Au template. As a proof of concept, we fabricated a large-area (1.2 cm × 2 cm) nanograting using the embedded structure. As shown in the atomic-force microscope (AFM) scan, the upper surface of the template was almost atomically flat (Figure 4B). The line width of the nanograting was 500 nm, and the half pitch of the grafting was 350 nm. After ERT, the Cu grating showed identical pattern period, and the line width was 550 nm. We repeated the ERT process with this nanotemplate for 50 times (Figure 4C). No significant damage to the nanostructure was observed and the AFM scans further confirmed that there were no measurable changes in the surface roughness of the template after 50 times of replication (Figure S10 and Table S4). SEM images with different magnifications help prove the successful fabrication of large-area nano-scale patterns (Figure S11). Apart from metal, nano-scale patterns deposited with metal oxide and conductive polymer could also be obtained (Figure S12). The embedded structure also allowed the fabrication of other nanostructures such as 200 nm dot arrays (half pitch 350 nm) and 50 nm gap arrays (half pitch 275 nm), as shown in Figure 4D.

We compare the resolution, throughput, and cost of ERT with several most commonly used patterning techniques (Figure 4E-4F and Table S5). Printing

techniques, such as inkjet and screen printings, are cost-effective for large-area fabrication particularly on flexible substrates. The roll-to-roll printing throughput is typically in the range of 1-10^3 m^2/h [9]. However, their patterning resolution are low, limiting to several tens of μm. High-resolution lithography techniques, such as photolithography, EBL, and NIL, can fabricate sub-10 nm patterns on planar and smooth rigid substrates. While applied on flexible substrates, the resolution is considerably deteriorated to sub-100 nm [17]. The throughputs of photolithography and NIL can reach ~1 m^2/h, while that of EBL is only 10^{-6}-10^{-4} m^2/h. Accordingly, the cost of patterning per area has been highly associated with the resolution capability of the patterning technique, being that higher cost for better resolution [18]. In contrast, ERT significantly outperforms the others because of its ability to disassociate the inter-dependent relationships among resolution, cost and throughput. As demonstrated above, ERT can readily fabricate sub-100 nm to many-μm features, and its throughput reach ~10^2 m^2/h regardless of the feature sizes of the patterns (detailed calculation shown in Table S5). In addition, ERT process is purely bottom up, it does not require expensive equipment, and its cost-per-area is similar to that of the existing printing technologies.

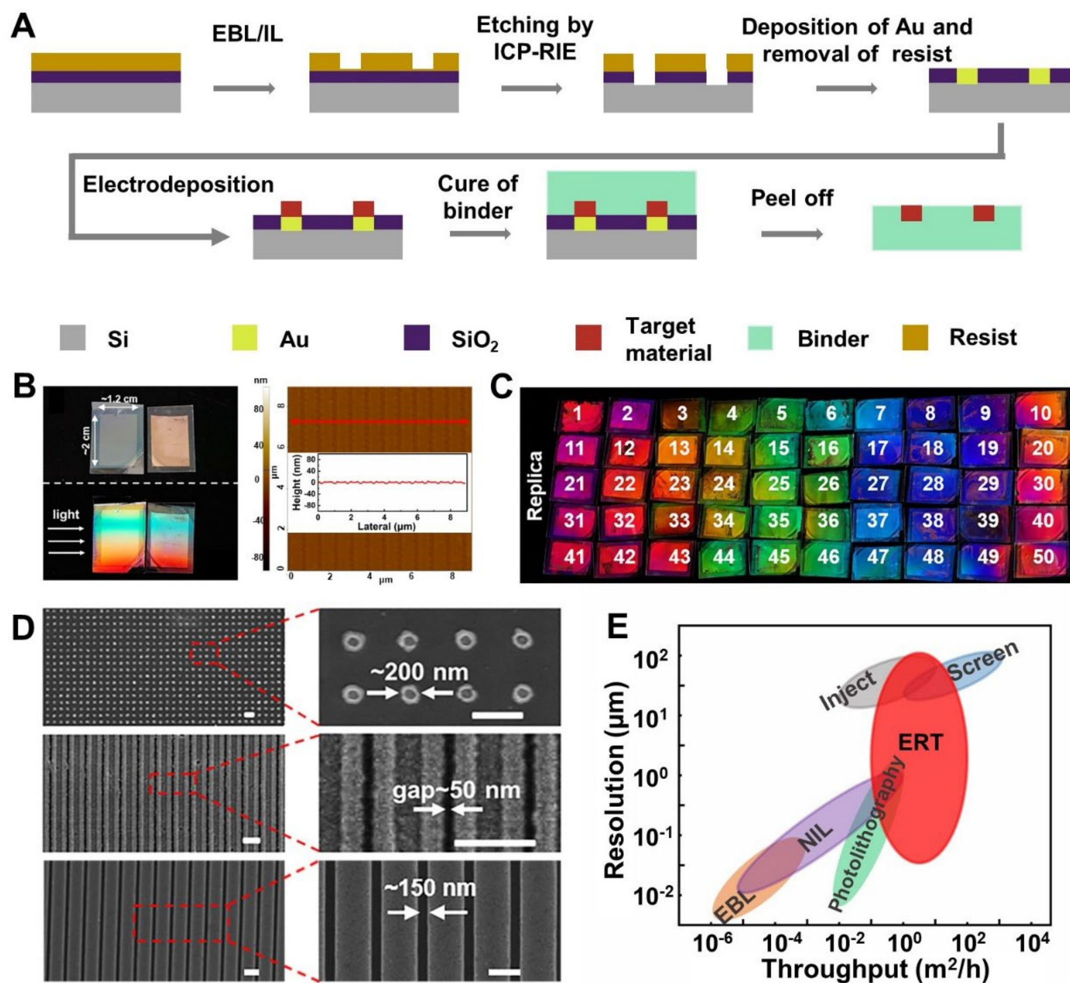

Figure 4. Fabrication of large-area nanoscale pattern by SiO_2-protecting structure template. (**A**) Fabrication process of ERT using SiO_2-protecting structure template. (**B**) Left: Large-area (2 cm × 1.2 cm) grating pattern template (left) and Cu pattern transferred to PET substrate (right). Right: AFM image of the grating pattern template. Inset: The height of the red line in the AFM image. (**C**) 50 replica samples fabricated by one template shown in Figure **B**. (**D**) SEM images of different nanoscale pattern. From up to down: Nanodots array with diameter of ~200 nm; Grating pattern with line width around 500 nm and gap around 50 nm; Grating pattern with line width around 550 nm and gap around 150 nm. Scale bar: 600 nm. (**E**) A comprehensive comparison of ERT with other typical conventional patterning techniques between resolution and throughput. The tilted ellipses for conventional patterning techniques indicate their resolution and throughput are dependent to each other, i.e., high resolution

accompanied by lower throughput. In contrast, the perpendicular ellipses for ERT indicate its resolution and throughput are independent to each other.

5. Applications of ERT for Flexible Electronic Devices

To illustrate the high flexibility and outstanding performance of the patterned materials via ERT, we fabricated embedded crossbar Cu meshes on PET as flexible transparent electrodes, which are indispensable components in a wide variety of flexible optoelectronic devices (Figure 5). In recent years, many kinds of alternative transparent electrodes have been widely studied to replace the brittle and expensive indium tin oxide (ITO) film [19]. Ag-based metal meshes made with printing and sintering are the most reported electrodes [20]. Herein we performed the ERT process to fabricate cost-effective Cu meshes (shown in Figure 5A). The sheet resistance (R_s) of as-made Cu mesh could easily reach 0.1 Ω/sq while its optical transmittance (T) was as high as 97%. The figure of merit (*FoM*) of the Cu meshes could be as high as ~25,650 (Figure S13), which far surpasses that of commercial ITO electrode on glass (R_s~10 Ω/sq, T~90%, *FoM*~348) and others (Figure 5B and Table S6) [21]. The embedded Cu meshes were also smooth, adhesive, flexible, and environmentally stable. The root means square height (S_q) over a large area of 9 mm^2 was only 17 nm (Figure S14). The resistance of Cu meshes maintained outstanding durability during 1000 bending tests, 100 Scotch tape tests, and the environmental stability tests in air, water, ethanol, and under high-temperature/high-humidity (85 °C/85%) over a period of 7 days (Figure S15).

With the outstanding optoelectronic properties and stability, we further used the metal meshes as transparent electrodes for several flexible devices including a flexible organic light emitting diodes, a flexible transparent heater, and a flexible touch screen, as shown in Figure 5C-5E. It should be noted that due to the ultrahigh FoM, the power consumption of the device was particularly low. For example, with an ultralow power density of ~0.3 W/cm^2, the temperature of the transparent heater reached as high as ~130 °C in 50 seconds (Figure 5D and S16).

We also demonstrated the applications of ERT for the fabrication of flexible electrochemical devices including a flexible organic electrochemical transistor (OECTs) and a flexible micro-supercapacitor (μSC). For the OECT, we fabricated the Au-based source/drain electrodes via ERT, followed by coating a layer of poly(3,4-ethylenedioxythiophene):poly(styrene sulfonate) (PEDOT:PSS) [22]. We tested the change of drain current (I_D) and the output and transfer characteristics indicate that the OECT worked well before and after 100 bending tests (Figure 5F). For the μSCs, we fabricated the interdigitated Au electrode arrays via ERT, followed by growth of MnO_2 on the Au areas to form a bilayer electrode. The Au layer acted as the current collector and the MnO_2 layer was used as the active material for the μSC device [23]. The current density-voltage (CV) measurements show that the flexible μSC possessed stable capacitive behavior (Figure 5G and S17). Furthermore, stretchable conductors could be realized using dissolvable PVA binder. Here a stretchable silver horseshoe pattern was transferred to a polydimethylsiloxane (PDMS) substrate. After 1,000 stretching cycles with 30% strain, the resistance change of the patterns didn't show a significant increase (Figure S18).

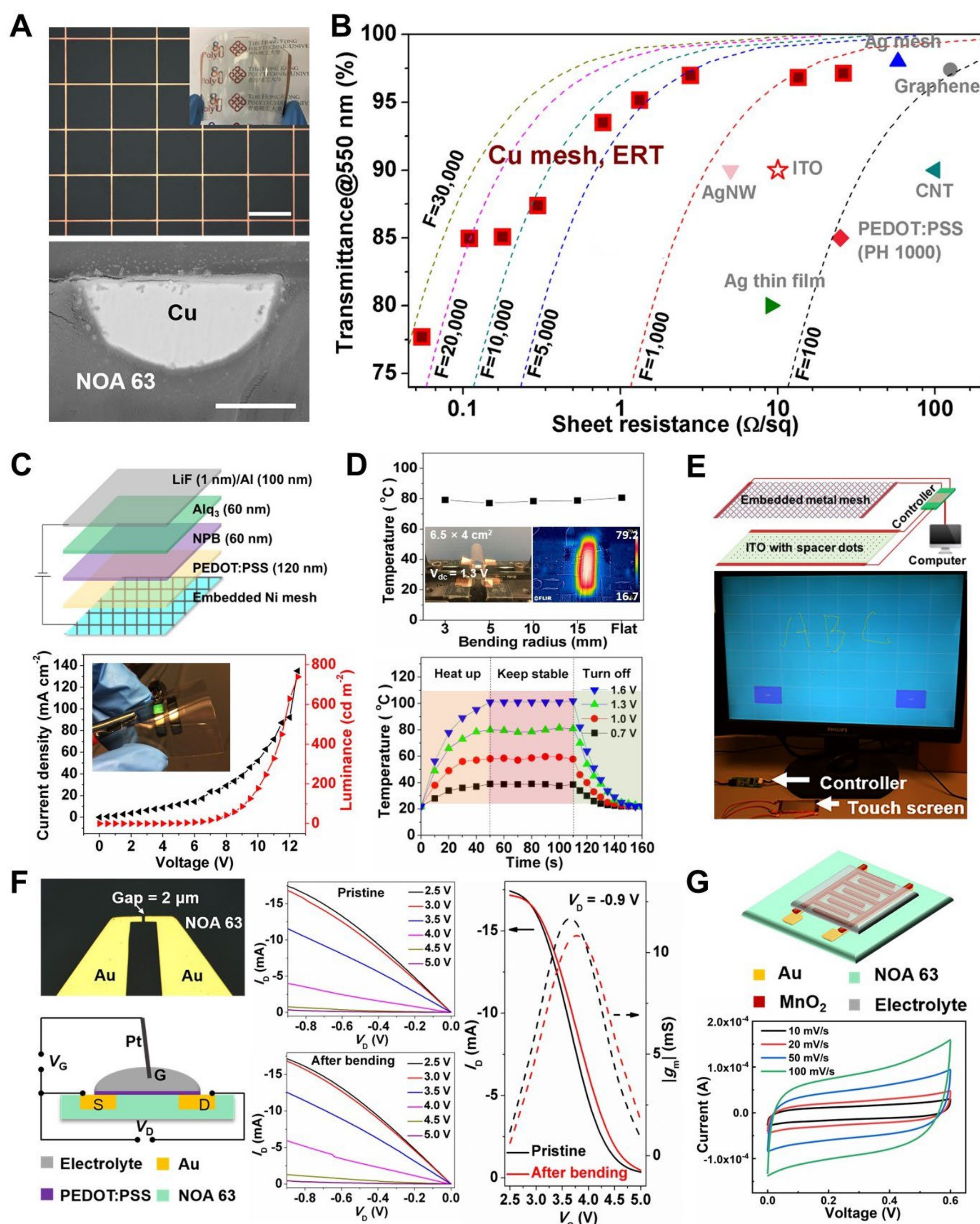

Figure 5. Demonstration of applications based on ERT. (**A**) Top: Optical microscopic image of Cu mesh fabricated by ERT process. Scale bar (pitch), 100 μm. Insert: Digital photograph of Cu-mesh-based flexible transparent electrode at bending state. Scale bar, 1 cm. Bottom: SEM image of cross-sectional view of ERT-based Cu line, embedded in the flexible substrate PET/NOA 63. Scale bar, 2 μm. (**B**) The optoelectronic properties (sheet resistance R_s, optical transmittance T, and figure of merit F) of as-made metal (Cu, Au, and Ni) meshes, compared with the performance of

other kinds of transparent electrode materials: the commercial ITO film, graphene, CNT network, commercial conductive polymer (PEDOT:PSS, PH 1000), AgNW network, Ag mesh fabricated by electrohydrodynamic (EHD) printing, and Ag ultrathin film. (**C**) Demonstration of flexible organic light-emitting diode (OLED) based on flexible transparent electrode (FTE). Top: Schematic illustration of green OLED device with Ni mesh-based FTEs. Bottom: Characterization of current density and luminance of OLED device. Insert, OLED device operation under bending state. (**D**) A flexible transparent heater (FTH) based on a 6.5×4.0 cm^2 ERT-based Cu mesh. Top: Temperature variation of flexible transparent heater (FTH) at a constant input voltage (1.3 V) while bended at different radii. The temperature of FTH keeps stable at ~80 ℃ during the bending test. The inserts are the digital image and IR image of FTH under bending state. Bottom: Temperature profile of FTH as a function of the time while applied with different voltages. (**E**) Demonstration of touch screen panel (TSP) assembled with an ERT-based metal mesh. Top: Schematic illustration of TSP using a top electrode of embedded Cu mesh and a bottom electrode of ITO with spacer array. Bottom: Demonstration of assembled TSP by writing letters ABC. (**F**) Left: Au source/drain electrodes with 2-μm channel length fabricated by ERT (top) and the schematic architecture of organic electrochemical transistor (OECT) (bottom). Middle: Output characteristics of as-assembled organic electrochemical transistor (OECT) device (top) before and (bottom) after mechanical bending. Right: transfer characteristics and associated transconductances of OECT device before and after mechanical bending. (**G**) Top: Demonstration of Micro supercapacitor (μSC) fabricated on PET by ERT. Au as the current collector, MnO_2 as the active material and 1 M Na_2SO_4 as aqueous electrolyte. Bottom: CV curves of MSC device under different scanning speed.

6. Conclusions

ERT provides a high-throughput and cost-effective approach to fabricating high-resolution functional structures on flexible substrate. ERT breaks the strong tradeoff between patterning resolution and cost per area in existing patterning technologies by introducing the electrochemical growth of materials on a pre-defined patterned mold.

Therefore, one can rapidly fabricate structures spanning from sub-100 nm to many cm in one experiment, while the materials to grow can be readily controlled by the electrochemical deposition chemistry. In this paper, we have demonstrated the patterning of different materials such as Cu, Ni, Au, Zn, MnO_2, CdS, PPy, and PANi. At the meanwhile, the transfer process of ERT addresses the challenge to fabricate large-area patterns on flexible substrates for flexible electronics and photonics. We have shown wafer-scale transfer of nano and micropatterns onto flexible substrates such as PET films, paper, and fabrics. Importantly, the structures fabricated on these flexible substrates by ERT are embedded in the substrate, so that the surface smoothness is exceedingly high in comparison to other bottom-up manufacture techniques. The high smoothness is critical for the application in optoelectronic devices. The embedded structure also benefits the high flexibility. At this moment, we demonstrate the applications of electrodes made with ERT for flexible OLED, transparent heater, touch screen, OECT and μSC. Thanks to the easy fabrication process and the versatility to many materials, we envision that ERT will be used for the fabrication of a wide variety of flexible electronic and photonic devices in the near future.

7. Experimental Section

7.1. Materials

Pure gold (Au, 99.999%, China New Metal), pure chromium (Cr, 99.9%, China New Metal, China), doped silicon wafer (Si, <100>, Suzhou Crystal Silicon Electronic & Technology CO., Ltd, China), Si wafer with silicon oxide layer (SiO_2, 30/300 nm, Suzhou Crystal Silicon Electronic & Technology CO., Ltd, China), positive photoresist (AZ 5214E, Microchemicals GmbH, Germany), developer for AZ 5214E (AZ 300 MIF, Microchemicals GmbH, Germany), negative photoresist (NR9-1500P, Futurrex, Inc., USA), developer for NR9-1500P (DR6, Futurrex, Inc., USA), positive photoresist (AZ MiR 701, MicroChemicals, GmbH), developer for AZ MiR 701 (AZ 726 MIF, MicroChemicals, GmbH), Au etchant (Transene Company, Inc.), methyl isobutyl ketone (99.5%, Sigma-Aldrich), chemicals for electron beam lithography (EBL): resist

ZEP520A, developer ZED-N50, and remover ZDMAC (Tokyo Zairyo Co., LTD.), acetone (99.9%, Sigma-Aldrich), ethanol (99.5%, Sigma-Aldrich), isopropanol (99.5%, Sigma-Aldrich), 1H,1H,2H,2H-Perfluorodecanethiol (PFDT, 97%, Sigma-Aldrich), commercial copper / gold / nickel / zinc plating solutions (Plug N Plate Cu Solution, Plug N Plate Au Solution, Plug N Plate Ni Solution, Plug N Plate Zn Solution, Caswell Inc., USA), cadmium nitrate tetrahydrate ($Cd(NO_3)_2 \cdot 4H_2O$, 99%, Uni-chem), sodium thiosulfate pentahydrate ($Na_2S_2O_3 \cdot 5H_2O$, 99.5%, Sigma-Aldrich), hydrochloric acid (HCl, >37%, Sigma-Aldrich), manganese(II) acetate tetrahydrate ($Mn(CH_3COO)_2 \cdot 4H_2O$, 99%, Sigma-Aldrich), sodium sulfate (Na_2SO_4, 99%, Acros), pyrrole (98%, Sigma-Aldrich), potassium nitrate (KNO_3, 99%, Uni-chem), aniline (99.5%, Acros), sulfuric acid (H_2SO_4, 99%, Sigma-Aldrich), Norland Optical Adhesive 63 (NOA 63, Norland Products Inc., USA), methyl methacrylate (MMA, 99%, Sigma-Aldrich), 2,2′-azobis(2-methylpropionitrile) (AIBN, 99%, Sigma-Aldrich), 4-hydroxybenzophenone (4-HOBP, 98%, Sigma-Aldrich), polyethylene terephthalate (PET, Suzhou Dawan Plastic Electronics Co. Ltd., China), poly(3,4-ethylenedioxythiophene):poly(styrene sulfonate) (PEDOT:PSS, Clevios™ PH 1000, Heraeous Epurio, Germany), polyvinyl alcohol (PVA, Mw 89,000-8,000, 99+% hydrolyzed, Sigma-Aldrich), hydrogen peroxide 30% (H_2O_2 30%, VWR International, Belgium), ammonium hydroxide solution, ($NH_3 \cdot H_2O$, 28% NH_3 in H_2O, ≥ 99.99% trace metals basis, Sigma-Aldrich). dodecyl triethoxy silane ($C_{18}H_{40}O_3Si$, Nanjing UP Chemical Co. Ltd., China), commercial polydimethylsiloxane (PDMS) membrane (200 μm, 1 mm, BALD advanced materials, China), Ecoflex 00-30 Soft platinum silicone liquid rubber (Bentley Advanced Materials, UK), soda-lime Glass (Kaivo Optoelectronic Technology Co. Ltd., China), glass sample bottle (KAISHIDE, China), poly(vinyl alcohol) 0588 low-viscosity (PVA-205, alcoholysis degree 87.0～89.0 mol/mol, Sigma-Aldrich).

7.2. Fabrication of Au-patterned templates for electrochemical replication

7.2.1. Photolithography

a) Etching process (Figure S1, left). A 5-nm-thickness adhesive Cr layer and a 25-nm-thickness Au layer were deposited by thermal evaporation on the Si or SiO_2 substrate. The positive photoresist AZ 5214 was spin-coated on the Au-coated substrate at 4000 rpm for 30 s. It was then pre-baked on a hotplate at 110 °C for 3 min. The photoresist was covered with the as-designed photomask and exposed under UV light with a dose of 40 mJ/cm^2 on a mask aligner (MA6, SUSS MicroTec, Germany). It was then post-baked at 90 °C for 1 min. The photoresist was then developed in the AZ 300 MIF developer for 70-80 s. The uncovered Au was then etched away in a mixed solution of pristine Au etchant and water at a 1:5 ratio for 60-120 s. The Au-pattern template was finally obtained after the photoresist was rinsed in acetone and ethanol and dried with compressed N_2. Au-patterned templates in Figure S6A and S6C were prepared through this etching process.

b) Lift-off process (Figure S1, middle). The bare Si or SiO_2 substrate was spin-coated with the negative photoresist NR9-1500P at 4000 rpm for 40 s. It was then pre-baked on a hotplate at 155 °C for 1 min. The photoresist was covered with the as-designed photomask and exposed under UV light with a dose of 170 mJ/cm^2 on the mask aligner MA6. It was then post-baked at 105 °C for 3 min. The photoresist was then developed in the DR6 developer for 10-15 s. The sample was rinsed in DI water and dried with compressed N_2. Subsequently, the photoresist-patterned substrate was deposited with a 5-nm-thickness adhesive Cr layer and a 25-nm-thickness Au layer by thermal evaporation. Finally, the photoresist and redundant deposited metals were washed away by acetone and ethanol. Au-patterned templates in Figure S6B and S6D were prepared through this lift-off process.

c) Interference lithography (IL) for the fabrication of nano-scale template (Figure 4A). The Si wafer with a 30 nm thickness of SiO_2 substrate was first treated with oxygen plasma (Harrick Plasma Cleaner, USA) for 5 minutes. Then the substrate was spin-coated with 800-nm-thick positive photoresist AZ MiR 701 at 3000 rpm and pre-baked at 90 °C for 60 s. The sample was exposed by a home-made interference lithography

system (HIL-1000, InterLitho Technology Limited, Hong Kong SAR) with a 405-nm laser. After post-baking at 110°C for 60 s, the photoresist was developed in the AZ 726 MIF developer for 60 s, and rinsing thoroughly with deionized water, gratings with 700 nm period and 200 nm linewidth were produced. Next, using the photoresist pattern as the etching mask, the underlying SiO_2 layer was directly etched using inductively coupled plasma reactive ion etching (ICP-RIE, Trion Phantom III, USA). The gas used is 40 sccm CF_4. The ICP power is 1500W and the RIE power is 32 W. The etching time is 30 s. After depositing a 5-nm-thickness adhesive Cr layer and a 25-nm-thickness Au layer by thermal evaporation, a lift-off process was performed with ultrasonic cleaning in RCA-1 solution ($NH_3{\cdot}H_2O$:H_2O_2:H_2O = 1:1:5) at 80 °C for 3 min, leaving the substate with periodic SiO_2/Au pattern.

7.2.2. E-beam lithography (EBL)

A bare Si substrate was spin-coated with the resist ZEP520A at 5200 rpm for 2 min. The patterning on resist was performed on EBL writer (JBX-9500FS Electron Beam Lithography System, JEOL Ltd., Japan). After post-baked at 180 °C for 3 min, the resist was developed in developer solution ZED-N50 for ~60 s. Subsequently, the sample was deposited with a 5-nm-thickness adhesive Cr layer and a 25-nm-thickness Au layer by thermal evaporation. Finally, the resist and redundant deposited metals were washed away by remover ZDMAC (lift-off route).

7.3. Electrochemical replication and transfer (ERT) process

The as-fabricated Au-patterned template was immersed in 5 mM PFDT ethanol solution for 10-15 min to form a self-assembled monolayer on the Au surface. The electrodeposition process could be carried out by the two-electrode setup on a source meter (Keithley 2400, Tektronix, Inc., USA) or the three-electrode setup on an electrochemical workstation (CHI 600e, CH Instruments, Inc., China). The SAM-modified Au-patterned template was used as the working electrode in the electrochemical deposition. The counter electrode could be the dissolvable pure target

material (such as Cu foil, Ni foil, or Zn foil) or noble platinum (Pt) foil. Ag/AgCl electrode was the reference electrode in the three-electrode setup. The details of electrodeposition solutions and other main parameters are listed in Table S1. After the target material deposited on the template, the template was rinsed by DI water and dried under compressed N_2.

7.3.1. Transfer step using NOA 63

NOA 63 could be cast on the template directly and cured under 365-nm UV light with a dose of more than 4,500 mJ/cm^2. The thickness is around 100 μm. Before the adhesive polymer NOA 63 was cured, the targeting substrate, such as cloth, paper, and PET film, was then directly placed and pressed on the NOA-cast substrate, which could help the adhesive polymer to peel off the target material pattern from the template. After the target material pattern was transferred, the Au-patterned template was rinsed with DI water and ethanol for reuse in the next fabrication.

7.3.2. Transfer step using PVA

PVA solution could be cast on the template directly and heated up at 80 °C for 20 min. The PVA layer with pattern then was peeled off from the template after solidification. After that, the PVA layer would be attached to the target substrate immediately. Finally, the PVA layer was fully dissolved using deionized water, through which the transferred pattern could be left on the surface of the target substrate.

7.4. Characterization techniques

Optical microscopic (OM) images were obtained on an optical microscope (Eclipse 80i, Nikon, Japan) with magnifications from 50× to 1000×.

Scanning electron microscopy (SEM) images were acquired on a field emission scanning electron microscope (FE-SEM, MIRA3, TESCAN, Czech Republic) with energy dispersive spectrometer (EDS, Oxford Instruments).

Atom force microscope (AFM, XE-100, Park Systems, Korea**)** was used to characterize the topography (line width, thickness, 3D view morphology, and surface roughness) of patterns.

X-ray diffraction (XRD) patterns were collected on an X-ray diffractometer (Rigaku SmartLab 9 kW, Japan) with a Cu Kα X-ray source.

Raman spectra were recorded on a Raman microscope (Nomadic^{TM} 3-in-1, BaySpec, USA), using the 532 nm laser.

Fourier transform infrared (FTIR) spectra were obtained on a FTIR spectrometer (Spectrum 100, PerkinElmer, USA).

X-ray photoelectron spectroscopy (XPS) data were collected on an X-ray photoelectron spectrometer (ESCALAB 250, Thermo Scientific, USA).

Contact angle (CA) was characterized on an optical contact angle measuring device (SDC-350, Dynetech, Inc., China) by dropping DI water on the sample surface.

Force vs. extension curve was recorded on a tensile strength tester (Instron 4411, Lab World Group, USA).

Sheet resistance (R_s) was tested by the four-probe method with a source meter (Keithley 2400 SourceMeter, Tektronix, Inc., USA).

Optical transmittance (T) was recorded on a UV-vis spectrometer (Cary 300, Varian, USA).

Bending tests were conducted on a stepper motor linear stage (TSA50-C, Zolix, China).

Infrared (IR) images were mapped by an IR camera (E4, FLIR, USA).

The transfer and output characteristics of the organic electrochemical transistor (OECT) were recorded on a four-probe station (Micromanipulator Probe station 450PM-B with Keithley 4200-SCS Semiconductor Parameter Analyzer, USA).

The current density-voltage-luminance (J-V-L) characteristics of OLED was performed on a Keithley 2400 SourceMeter and a spectroradiometer (SpectraScan® PR-650, Photo Research, USA).

Electrochemical performance of the micro-supercapacitor was characterized on an electrochemical workstation (CHI 600e, CH Instruments, Inc., China).

Movies and digital images were recorded by a single-lens reflex camera (D7200, Nikon, Japan).

Supporting Information

Supporting Information is available from the Wiley Online Library or from the author.

Acknowledgments

We acknowledge the financial support from the State Key Laboratory of Ultra-precision Machining Technology (1-BBXR) and RGC Senior Research Fellow Scheme (SRFS2122-5S04).

Author contributions:

Conceptualization: XL, ZJC, ZJZ

Idea discussion: XL, ZJC, ZJZ, JC, DRW

Experiment: XL, ZJC, HXW, WSW, S-WN, MMR, PL, QYH, GZF, JWZ

Supervision: ZJZ, WDL.

Data analysis: XL, ZJC, ZJZ

Writing-original draft: XL, ZJZ

Writing-review & editing: XL, ZJC, QYH, ZJZ

Competing interests:

Authors declare no competing interests.

References

[1] a) D. H. Kim, N. S. Lu, R. Ma, Y. S. Kim, R. H. Kim, S. D. Wang, J. Wu, S. M. Won, H. Tao, A. Islam, K. J. Yu, T. I. Kim, R. Chowdhury, M. Ying, L. Z. Xu, M. Li, H. J. Chung, H. Keum, M. McCormick, P. Liu, Y. W. Zhang, F. G. Omenetto, Y. G.

Huang, T. Coleman, J. A. Rogers, *Science* **2011**, 333, 838; b) H. Zhang, J. A. Rogers, *Adv. Opt. Mater.* **2019**, 7, 1800936; c) N. L. Rosi, C. A. Mirkin, *Chem. Rev.* **2005**, 105, 1547; d) L. Chen, C. Yan, Z. Zheng, *Mater. Today* **2018**, 21, 38; e) J. Kathirvelan, *Sensor Rev* **2021**, 41, 46; f) G. Q. Liu, M. M. Rong, H. Hu, L. A. Chen, Z. Xie, Z. J. Zheng, *Adv. Mater. Technol.* **2022**, 7, 2101493.

[2] I.-C. Cheng, S. Wagner, in *Flexible Electronics*, Vol. 11 (Eds: A. Salleo, W. S. Wong), Springer, Boston, USA **2009**, Cp. 1.

[3] C. Mack, *Fundamental Principles of Optical Lithography: the Science of Microfabrication*, John Wiley & Sons, West Sussex, UK, **2008**.

[4] C. Vieu, F. Carcenac, A. Pépin, Y. Chen, M. Mejias, A. Lebib, L. Manin-Ferlazzo, L. Couraud, H. Launois, *Appl. Surf. Sci.* **2000**, 164, 111.

[5] S. Y. Chou, P. R. Krauss, P. J. Renstrom, *Science* **1996**, 272, 85.

[6] a) D.-Y. Khang, H. Jiang, Y. Huang, J. A. Rogers, *Science* **2006**, 311, 208; b) A. Carlson, A. M. Bowen, Y. Huang, R. G. Nuzzo, J. A. Rogers, *Adv. Mater.* **2012**, 24, 5284; c) H. E. Lee, S. Kim, J. Ko, H.-I. Yeom, C.-W. Byun, S. H. Lee, D. J. Joe, T.-H. Im, S.-H. K. Park, K. J. Lee, *Adv. Funct. Mater.* **2016**, 26, 6170; d) G. Y. Liu, Z. Tian, Z. Y. Yang, Z. Y. Xue, M. Zhang, X. D. Hu, Y. Wang, Y. K. Yang, P. K. Chu, Y. F. Mei, L. Liao, W. D. Hu, Z. F. Di, *Nat. Electron.* **2022**, 5, 275; e) Z. J. Ma, Q. Y. Huang, Q. Xu, Q. N. Zhuang, X. Zhao, Y. H. Yang, H. Qiu, Z. L. Yang, C. Wang, Y. Chai, Z. J. Zheng, *Nat. Mater.* **2021**, 20, 859; f) C. P. Zhang, J. X. Cai, C. W. Liang, A. Khan, W. D. Li, *Adv. Funct. Mater.* **2019**, 29, 1903123.

[7] a) K. B. Ozutemiz, C. Majidi, O. B. Ozdoganlar, *Adv. Mater. Technol.* **2022**, 7, 2200295; b) E. P. Yalcintas, K. B. Ozutemiz, T. Cetinkaya, L. Dalloro, C. Majidi, O. B. Ozdoganlar, *Adv. Funct. Mater.* **2019**, 29, 1906551 .

[8] a) S. Cabrini, S. Kawata, *Nanofabrication Handbook*, CRC Press, Boca Raton, FL, USA, **2012**; b)P. van Assenbergh, E. Meinders, J. Geraedts, D. Dodou, *Small* **2018**, 14, 1703401.

[9] D. M. Tennant, in *Nanotechnology*, Ed: G. Timp, Springer, New York, NY, USA **1999**, Cp. 4.

[10] a) K. Suganuma, *Introduction to Printed Electronics*, Vol. 74, Springer, New York, NY, USA, **2014**, Cp. 1; b)Y. N. Xia, G. M. Whitesides, *Annu. Rev. Mater. Sci.* **1998**, 28, 153.

[11] B. E. Kahn, *Proc. IEEE* **2015**, 103, 497.

[12] a) G. Hu, J. Kang, L. W. Ng, X. Zhu, R. C. Howe, C. G. Jones, M. C. Hersam, T. Hasan, *Chem. Soc. Rev.* **2018**, 47, 3265; b) K. Fukuda, T. Someya, *Adv. Mater.* **2017**, 29, 1602736.

[13] a) B. D. Gates, Q. B. Xu, M. Stewart, D. Ryan, C. G. Willson, G. M. Whitesides, *Chem. Rev.* **2005**, 105, 1171; b) Y. N. Xia, G. M. Whitesides, *Angew. Chem. Int. Edit.* **1998**, 37, 550; c) D. Qin, Y. N. Xia, G. M. Whitesides, *Nat. Protoc.* **2010**, 5, 491; d) D. W. Wang, S. G. Thomas, K. L. Wang, Y. N. Xia, G. M. Whitesides, *Appl. Phys. Lett.* **1997**, 70, 1593.

[14] a) G. Q. Liu, M. Hirtz, H. Fuchs, Z. J. Zheng, *Small* **2019**, 15, 1904507; b) G. Q. Liu, S. H. Petrosko, Z. J. Zheng, C. A. Mirkin, *Chem. Rev.* **2020**, 120, 6009; c) F. W.

Huo, Z. J. Zheng, G. F. Zheng, L. R. Giam, H. Zhang, C. A. Mirkin, *Science* **2008**, 321, 1658; d) R. D. Nagel, T. Haeberle, M. Schmidt, P. Lugli, G. Scarpa, *Nanoscale Res. Lett.* **2016**, 11, 143.
[15] a) T. N. Kim, K. Campbell, A. Groisman, D. Kleinfeld, C. B. Schaffer, *Appl. Phys. Lett.* **2005**, 86, 201106; b) P. D. Yang, T. Deng, D. Y. Zhao, P. Y. Feng, D. Pine, B. F. Chmelka, G. M. Whitesides, G. D. Stucky, *Science* **1998**, 282, 2244.
[16] a) Y. Yourdshahyan, H. K. Zhang, A. M. Rappe, *Phys. Rev. B* **2001**, 63, 081405; b) H. Notsu, W. Kubo, I. Shitanda, T. Tatsuma, *J. Mater. Chem.* **2005**, 15, 1523.
[17] a) K. Scholten, E. Meng, *Microsyst. Nanoeng.* **2016**, 2, 16053; b) S. H. Ahn, L. J. Guo, *Adv. Mater.* **2008**, 20, 2044.
[18] a) G. D. Hutcheson, presented at *Extreme Ultraviolet (EUV) Lithography IX*, **2018**; b) D. S. Engstrom, B. Porter, M. Pacios, H. Bhaskaran, *J. Mater. Res.* **2014**, 29, 1792.
[19] a) D. S. Hecht, L. B. Hu, G. Irvin, *Adv. Mater.* **2011**, 23, 1482; b) A. Khan, C. W. Liang, Y. T. Huang, C. P. Zhang, J. X. Cai, S. P. Feng, W. D. Li, *Adv. Eng. Mater.* **2019**, 21, 1900723; c) A. Khan, S. Lee, T. Jang, Z. Xiong, C. P. Zhang, J. Y. Tang, L. J. Guo, W. D. Li, *Small* **2016**, 12, 3021.
[20] a) M. G. Kang, L. J. Guo, *Adv. Mater.* **2007**, 19, 1391; b) L. Li, B. Zhang, B. Zou, R. Xie, T. Zhang, S. Li, B. Zheng, J. Wu, J. Weng, W. Zhang, W. Huang, F. Huo, *ACS Appl. Mater. Inter.* **2017**, 9, 39110.
[21] R. B. H. Tahar, T. Ban, Y. Ohya, Y. Takahashi, *J. Appl. Phys.* **1998**, 83, 2631.
[22] D. Khodagholy, J. Rivnay, M. Sessolo, M. Gurfinkel, P. Leleux, L. H. Jimison, E. Stavrinidou, T. Herve, S. Sanaur, R. M. Owens, G. G. Malliaras, *Nat. Commun.* **2013**, 4, 2133.
[23] X. Zhang, D. D. Zhao, Y. Q. Zhao, P. Y. Tang, Y. L. Shen, C. L. Xu, H. L. Li, Y. Xiao, *J. Mater. Chem. A* **2013**, 1, 3706.

A new additive patterning technique, named electrochemical replication and transfer (ERT), is developed to pattern a wide variety of metals, semiconductors, and polymers with resolutions spanning from sub-100 nm to many cm on flexible substrates at low cost and high throughput.

Zijian Chen, Xi Lu, Huixin Wang, Jian Chang, Dongrui Wang, Wenshuo Wang, Sze-Wing Ng, Mingming Rong, Peng Li, Qiyao Huang, Jianwen Zhong, Zhuofei Gan, Wen-Di Li, Zijian Zheng*

Electrochemical replication and transfer for low-cost, sub-100 nm patterning of materials on flexible substrates

Electrodeposition of target material
(i) Au@Si
(ii) X@Au@Si
Cast and cure of UV-curable binder
Transfer of target material pattern
Reuse of Au-patterned template
PFDT@Au
(iii) S@X@Au@Si
(iv) X@S
Au
Si wafer
Target material (X)
Flexible substrate with binder (S)
PFDT

Supporting Information

Electrochemical replication and transfer for low-cost, sub-100 nm patterning of materials on flexible substrates

*Zijian Chen, Xi Lu, Huixin Wang, Jian Chang, Dongrui Wang, Wenshuo Wang, Sze-Wing Ng, Mingming Rong, Peng Li, Qiyao Huang, Jianwen Zhong, Zhuofei Gan, Wen-Di Li, Zijian Zheng**

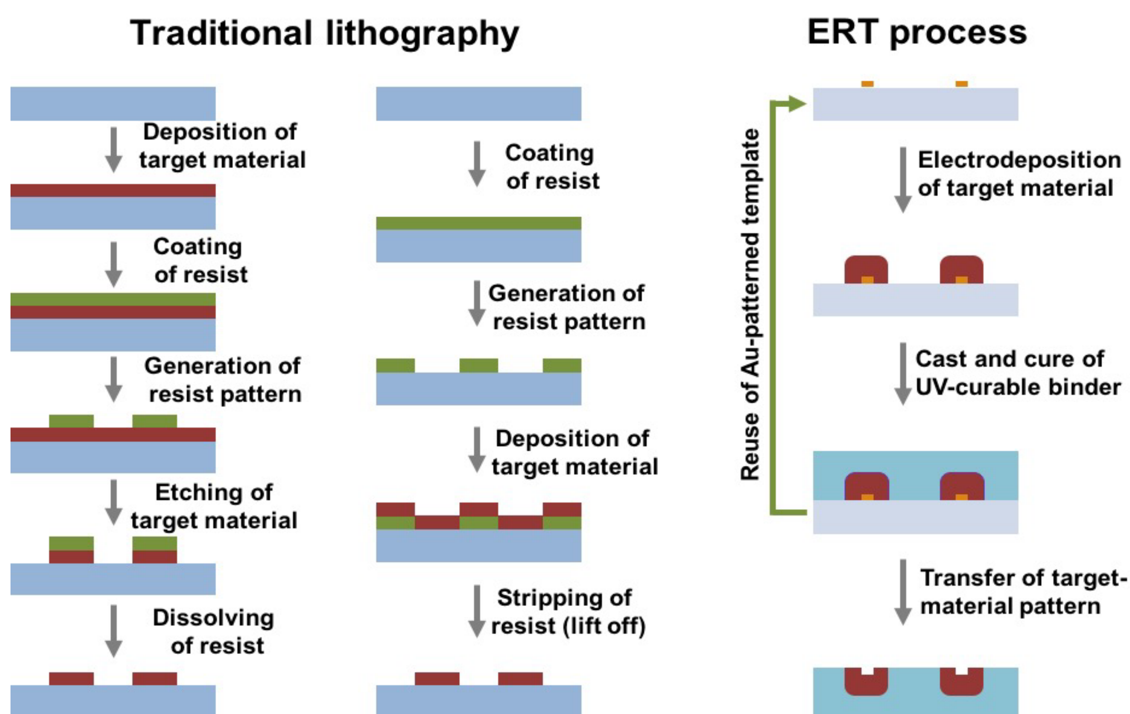

Figure S1. Comparison of traditional lithography and ERT process. In traditional lithography, the pattern of target material cannot be obtained directly. We need to firstly create the pattern on the resist, and then using this patterned resist to transfer the pattern onto the target material through etching or lift-off process. In ERT process, the pattern of target material is replicated on the template directly, without any resist assistance and redundant materials.

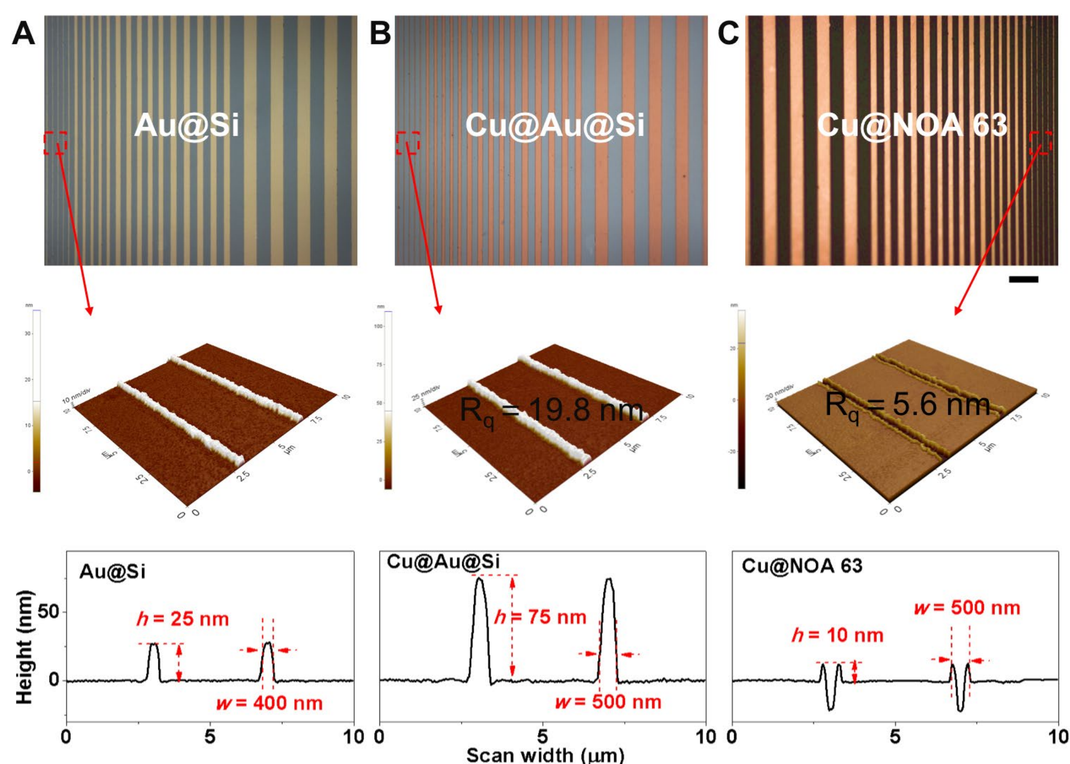

Figure S2. Characterization of ERT process based on a parallel-line pattern. Top, optical microscopic images. Middle, 3D images of topographic images characterized by AFM. Bottom, the profiles of pattern lines during ERT process. (**A**) Au-pattern template (Au@Si). Height of Au is about 25 nm. Linewidth is about 400 nm. (**B**) Cu deposited on Au-pattern template (Cu@Au@Si). Thickness of deposited Cu is about 50 nm (by subtracting 25-nm thickness of Au layer from the total 75-nm thickness). Linewidth is about 500 nm. Current density, 2 mA/cm^2. electrodeposition time, 1 min. (**C**) Cu pattern transferred into the NOA 63 substrate (Cu@NOA 63). Height of transferred Cu line based on the NOA 63 substrate surface is about 10 nm (mostly embedded in the PET/NOA 63 substrate). Linewidth is about 500 nm. The phenomenon of Cu embedded in the PET/NOA 63 substrate can significantly reduce the surface roughness, where root-mean-square roughness (R_q) is reduced to 5.6 nm from 19.8 nm.

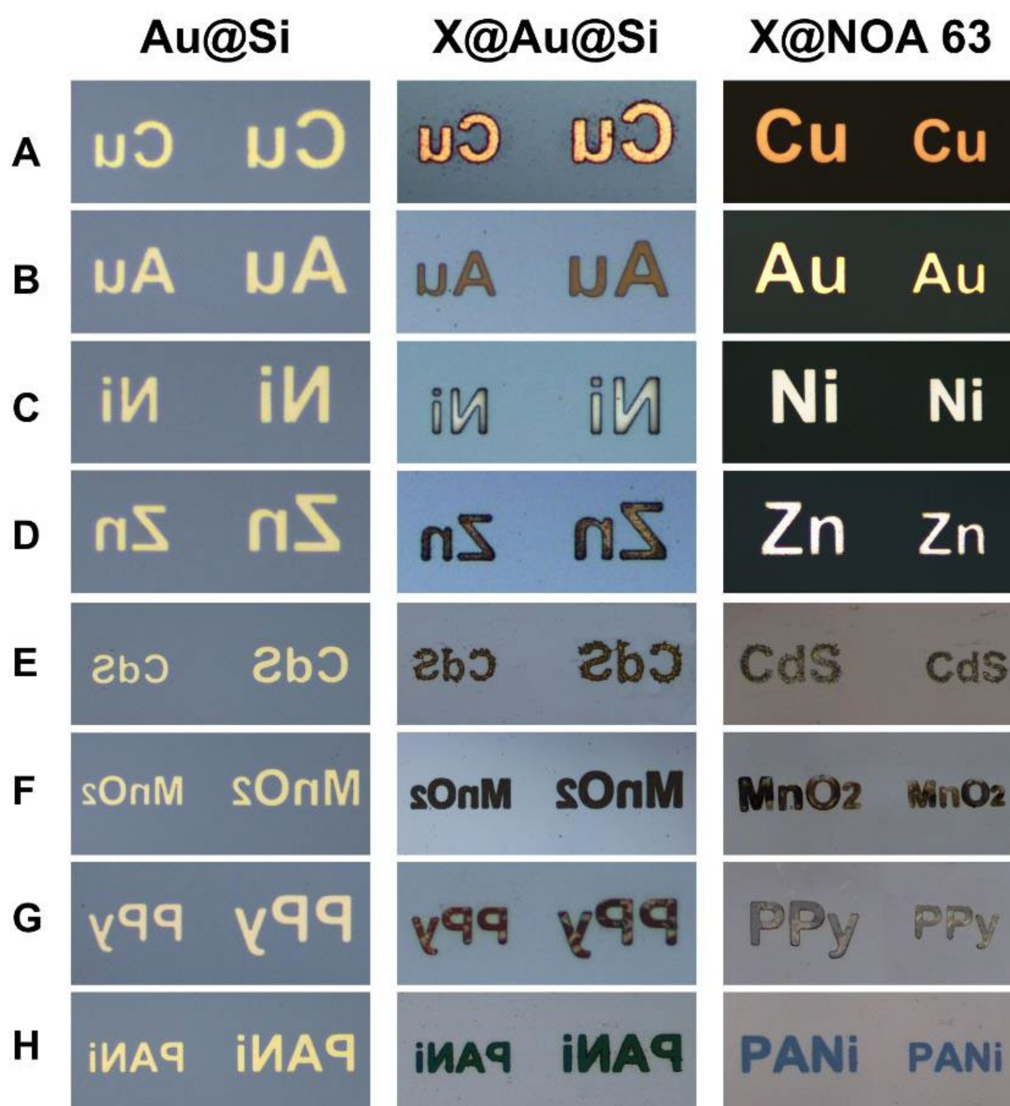

Figure S3. Optical microscopic images of different patterns based on eight different materials during ERT processes. (**A**) Cu, (**B**) Au, (**C**) Ni, (**D**) Zn, (**E**) CdS, (**F**) MnO_2, (**G**) PPy, (**H**) PANi. Left column, Au-patterned templates (Au@Si). Middle column, different target materials deposited on the Au-patterned templates (X@Au@Si). Right column, different target material pattern transferred into the target substrates PET/NOA 63 (X@NOA 63). Scale bar, 100 µm.

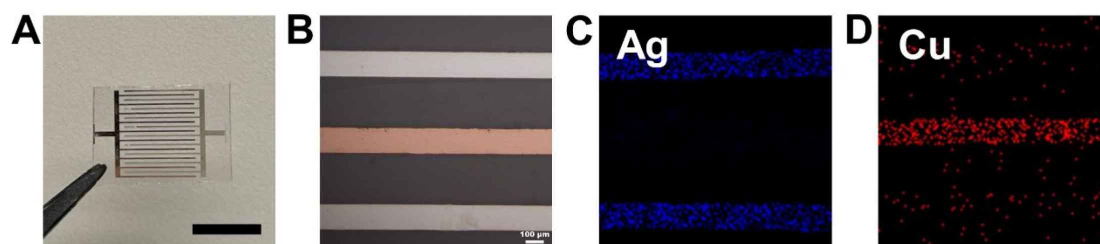

Figure S4. Interdigital electrode pattern deposited with different materials on one substrate. (**A**) Digital photo of the Ag-Cu interdigital electrode pattern. Scale bar: 1 cm. (**B**) Optical image of the interdigital electrodes deposited with Ag and Cu. (**C**) EDX mapping of Ag element. (**D**) EDX mapping of Cu element.

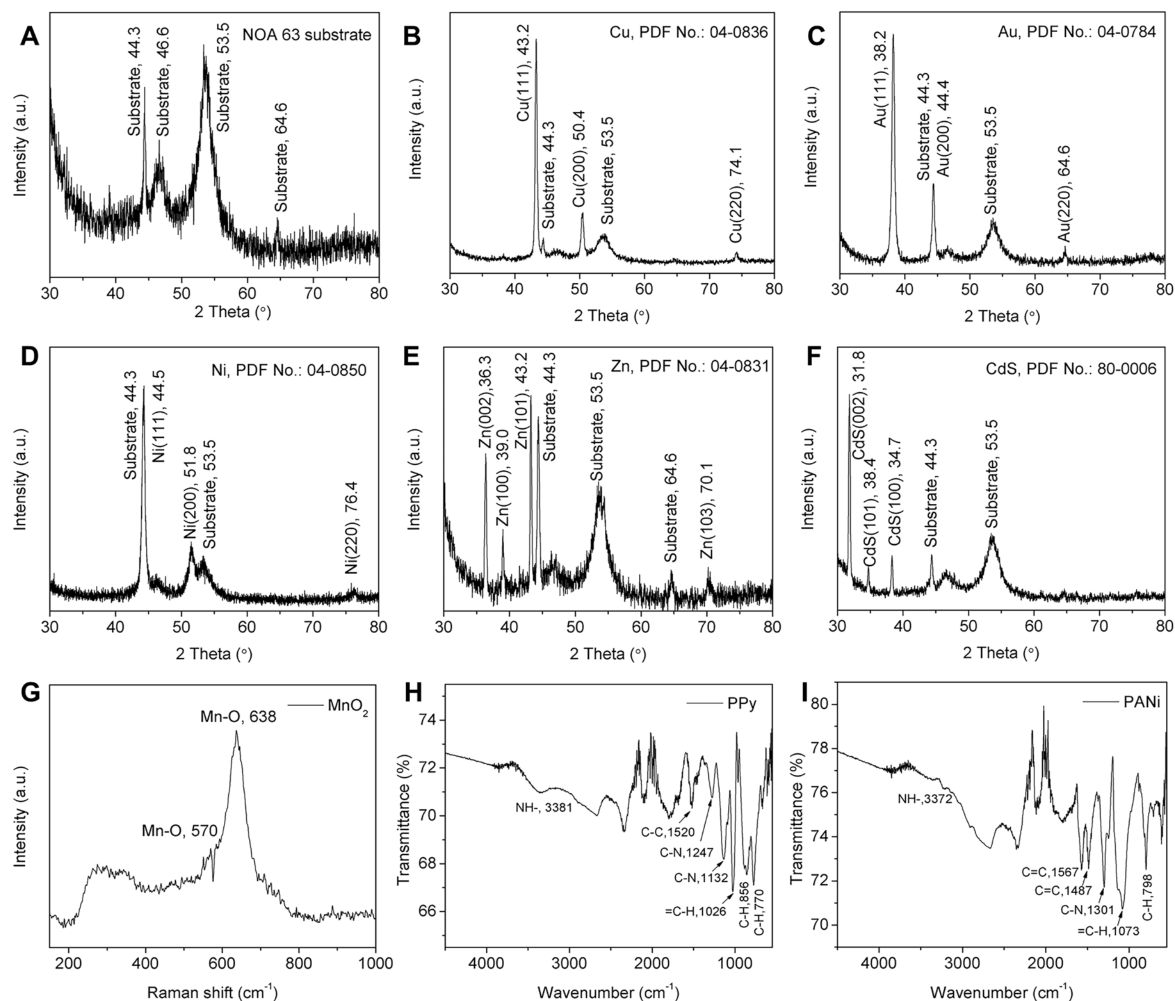

Figure S5. Characterization of eight materials fabricated by ERT method. XRD patterns of (**A**) Substrate (PET/NOA63), (**B**) Cu, (**C**) Au, (**D**) Ni, (**E**) Zn and (**F**) CdS. Raman spectrum of (**G**) MnO_2. FTIR spectra of (**H**) PPy and (**I**) PANi.

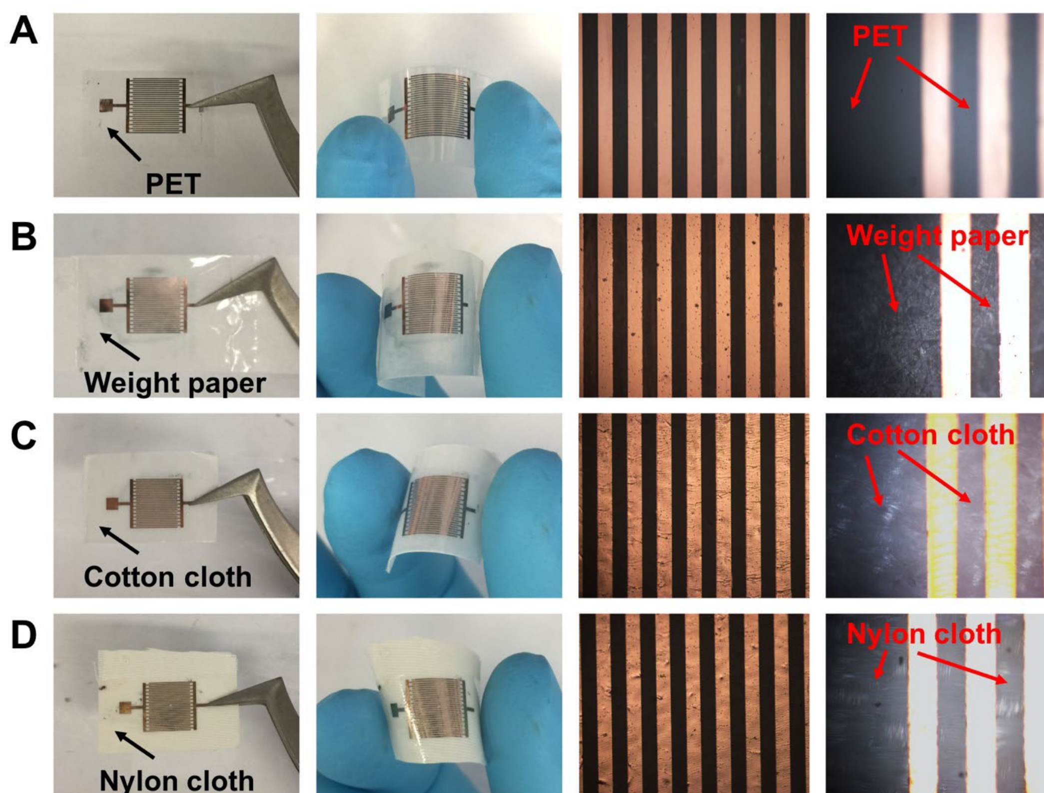

Figure S6. ERT method applicable to various flexible and wearable substrates: (A) PET, (B) paper, (C) cotton, and (D) nylon clothes. UV-curable binder for the four substrates is all NOA 63. Current density, 2 mA/cm^2. Electrodeposition time, 10 min. The first column: flat state of ERT-based interdigital electrodes on the four substrates. Scale bar, 5 mm. The second column: bending state of ERT-based interdigital electrodes on the four substrates. Scale bar, 5 mm. The third column: optical microscopic images of Cu patterns. Scale bar, 300 µm. The fourth column: optical microscopic images focusing on the surfaces of the four substrates. PET film is flat. The textures of paper, cotton, and nylon clothes are observed. Scale bar, 150 µm.

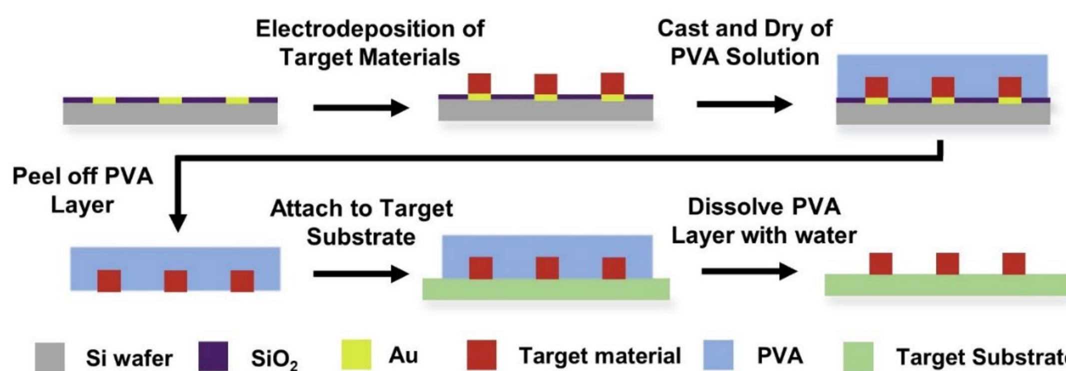

Figure S7. Illustration showing the fabrication process of using PVA as the binder for arbitrary transfer. Before the electrodeposition step, the Au pattern was fabricated by photolithography, and the surface of the Au patterns was modified with PFDT.

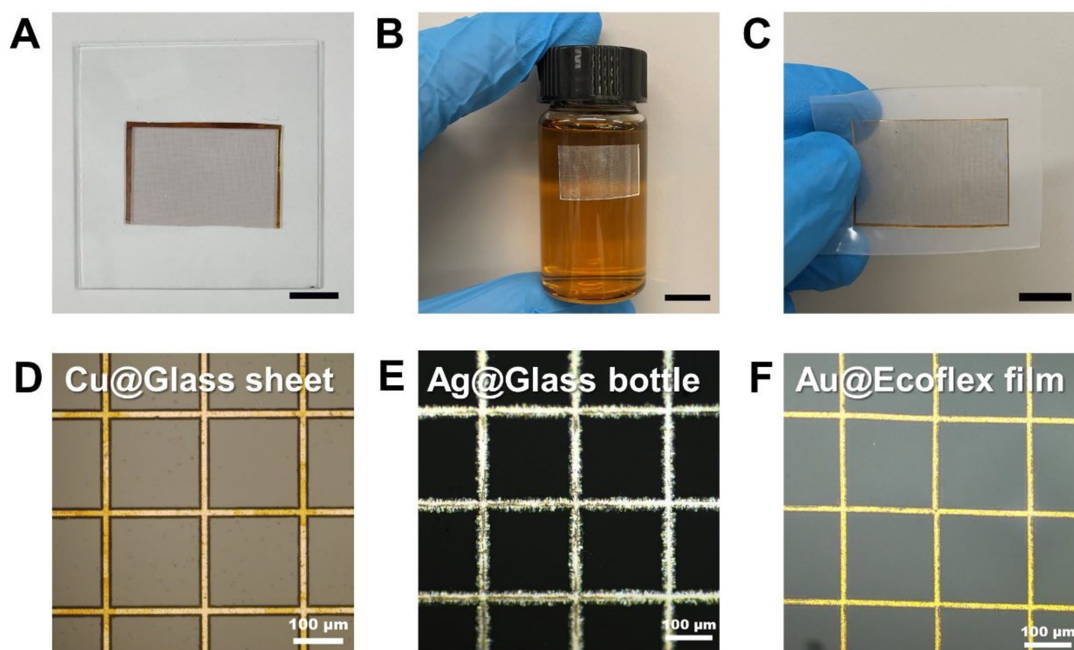

Figure S8. Transfer of patterns with various materials to different substrate. (**A**) Cu grid pattern on hard substrates-glass sheet. (**B**) Ag grid pattern on curved substrates-glass bottle. (**C**) Au grid pattern on stretchable substrates-Ecoflex. Scale bar: 1cm. (**D**) Optical images of Au Cu grid pattern on glass sheet. (**E**) Ag grid pattern on glass bottle. (**F**) Au grid pattern on Ecoflex film.

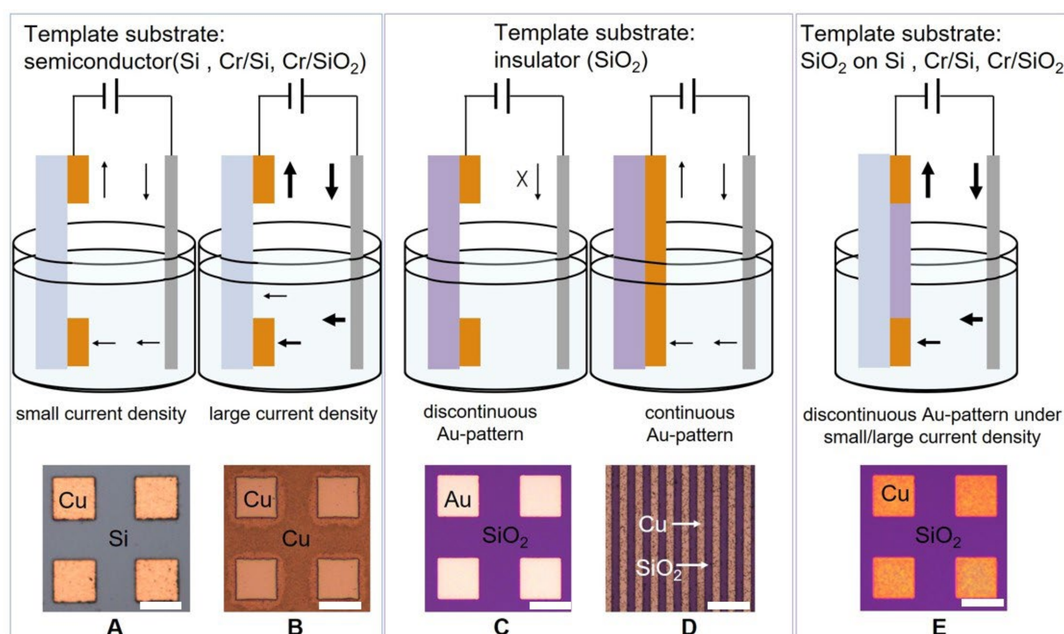

Figure S9. A summary of the mechanism of electrochemical replication, schematically illustrated by equivalent circuit diagrams and optical microscopic images on different Au-patterned templates and under different current densities. For the templates using semiconducting materials as substrates (Si, Cr/Si, or Cr/SiO_2), target material can be site-selectively deposited on the Au pattern and form high quality pattern under optimized current density (**A**,1.0 - 2.0 mA/cm^2), while cannot form pattern effectively under relatively large current density (**B**, >2.0 mA/cm^2). For the template using non-conductive material as substrate (SiO_2), the target material cannot be deposited on the separated island-type pattern (**C**), while can be deposited on the continuous pattern (**D**). For the SiO_2-protecting template which combines the SiO_2 and semiconductor layer, the target materials can be deposited successfully on the separated island-type pattern under both small and large current density situation (**E**). Scale bar: 50 μm.

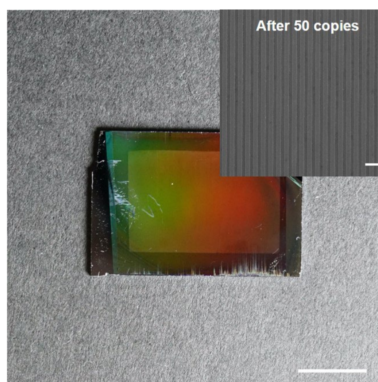

Figure S10. Nanoscale grating pattern template after 50 times of fabrication. Scale bar: 1 cm. Inset image: SEM image of Au-patterned templated after used in ERT processes for 50 copies. Scale bar: 1 µm.

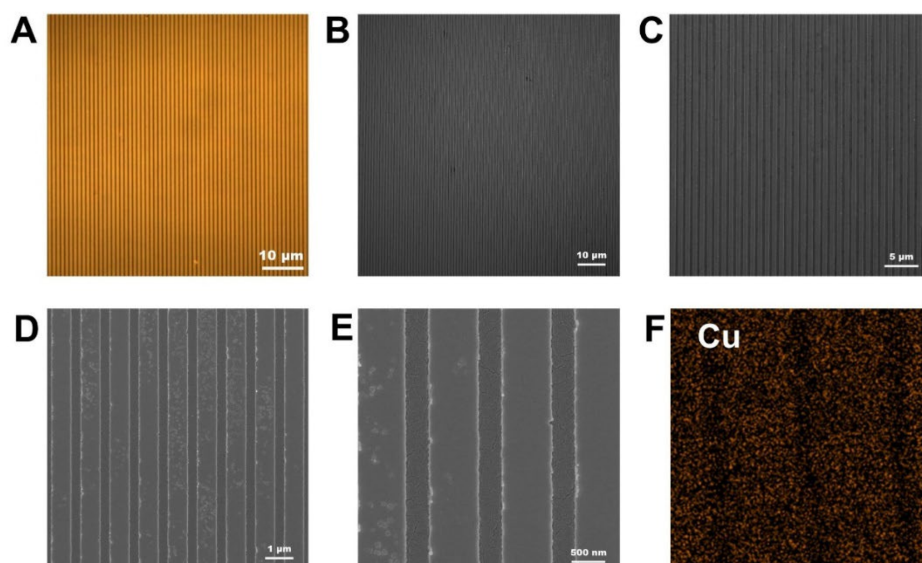

Figure S11. Characterization of large-area nanoscale grating pattern. (**A**) Optical image. (**B-E**) SEM images with different magnification. (**F**) EDX result of Cu element taken from (**E**).

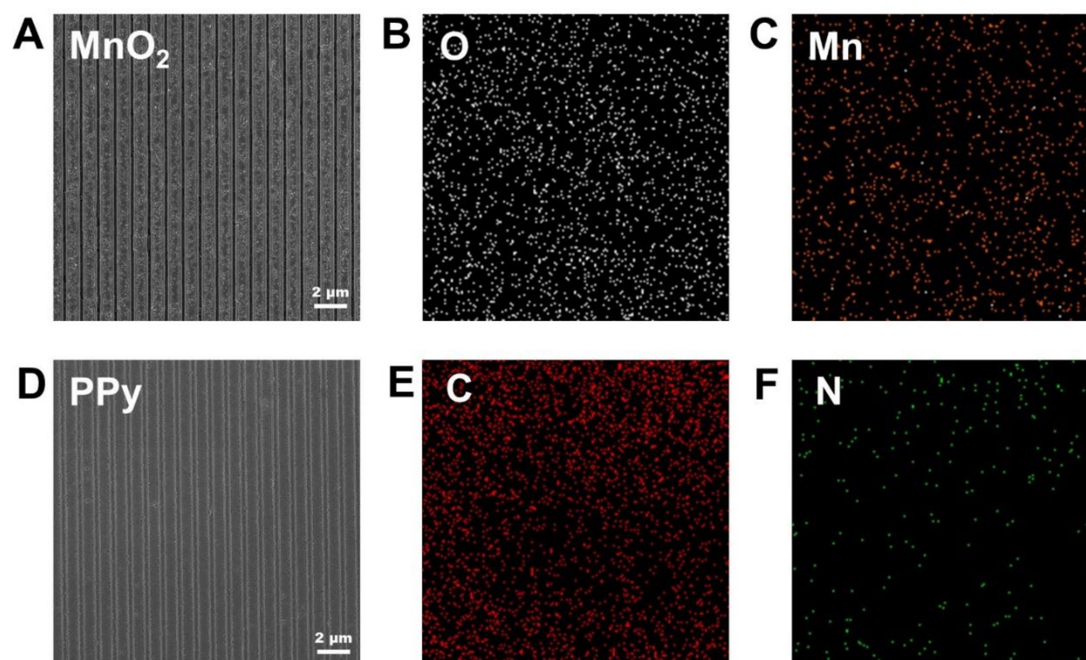

Figure S12. Fabrication of nano scale grating pattern with metal oxide and conductive polymer. (**A**) SEM image of MnO_2 grating pattern. (**B**) EDX result of O element taken from (**A**). (**C**) EDX result of Mn element taken from (**A**). (**D**) SEM image of PPy grating pattern. (**E**) EDX result of C element taken from (**D**). (**F**) EDX result of N element taken from (**D**).

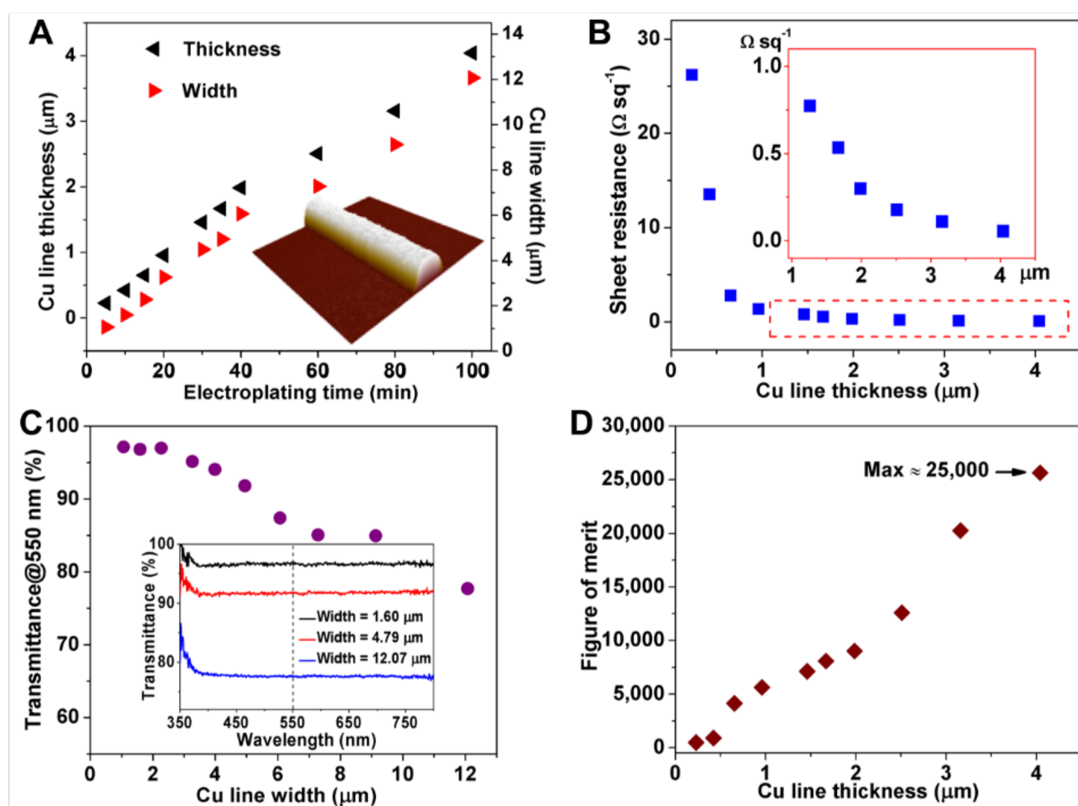

Figure S13. (**A**) Line thickness and width of Cu mesh versus electrodeposition time. The thickness and width of lines increase with the increasing the electrodeposition time. Inset: AFM image of Cu mesh on Au-patterned template. The thickness and width of lines were measured by AFM. Optoelectronic performance of Cu mesh-based FTEs: (**B**) sheet resistance, (**C**) optical transmittance, and (**D**) figure of merit (*FoM*) of embedded Cu mesh-based FTEs. The conductivity and *FoM* of metal mesh increase with the increasing electrodeposition time, whereas the transmittance decreases as expected.

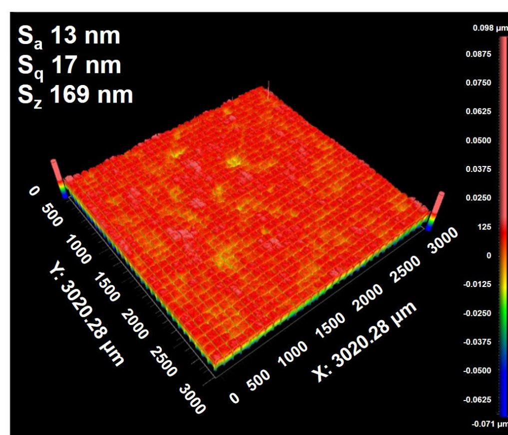

Figure S14. Optical Surface Profiler test of ERT-based Cu meshes. The area is 9 mm^2. For the surface roughness, the arithmetic mean height (S_a) is 13 nm, the root mean square height (S_q) is 17 nm and the maximum height difference (S_z) is 169 nm.

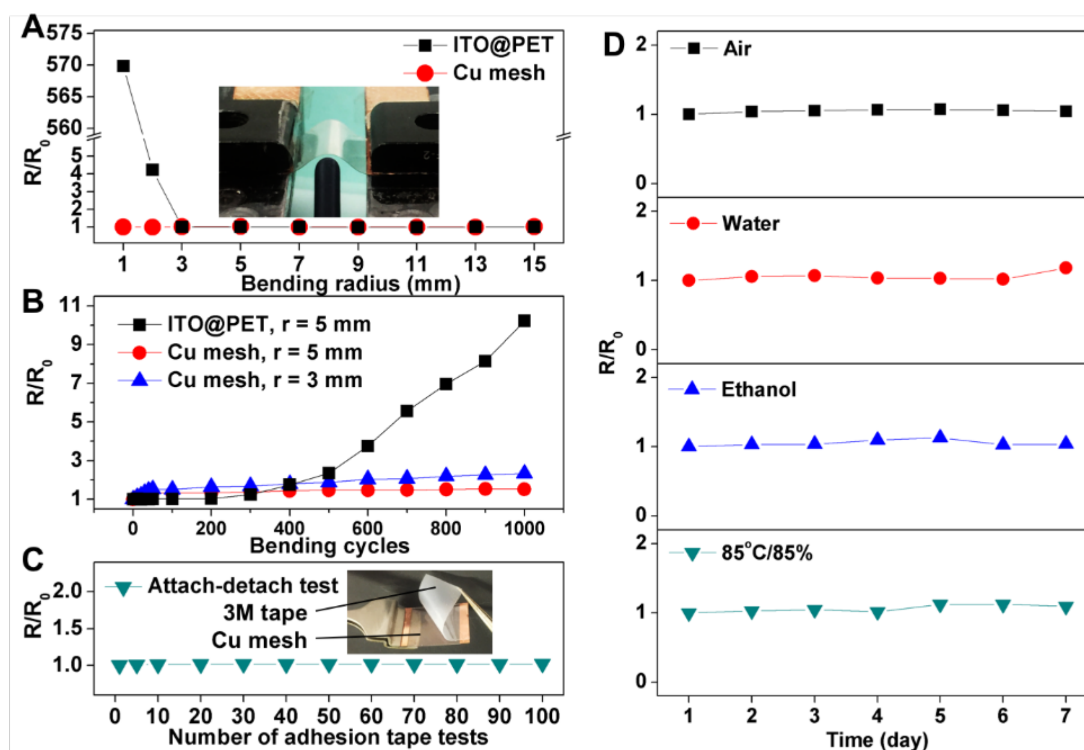

Figure S15. Mechanical flexibility and environmental stability of ERT-based Cu meshes. Resistance variations of Cu mesh-based FTEs and ITO film deposited on PET substrate (ITO@PET, control group) bended at different radii (**A**) and bending cycles (**B**). (**C**) Normalized resistance of Cu mesh-based FTE during 100-cycle attach-detach tests for investigation of the adhesion between Cu mesh and NOA 63/PET substrate. (**D**) Normalized resistance of Cu mesh-based FTEs in four typical environments for 7 days, including air, water, ethanol, and high-temperature/high-humidity (85 °C/85%) conditions.

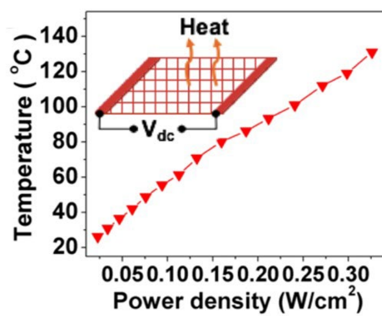

Figure S16. Maximum temperature of FTH as a function of the supplied power density.

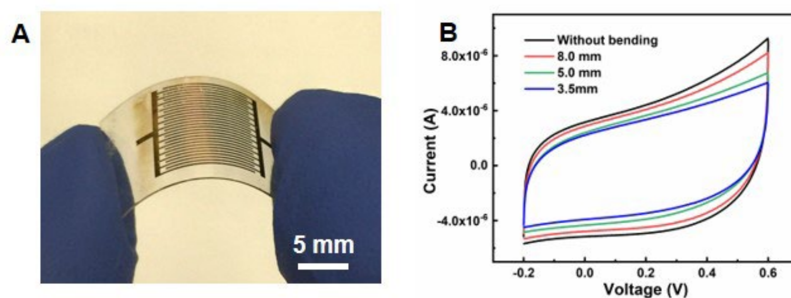

Figure S17. (**A**) Illustration of a μSC fabricated on a flexible PET substrate by ERT. (**B**) CV test of MnO_2/Au μSC device with PVA/LiCl as electrolyte under different bending radius.

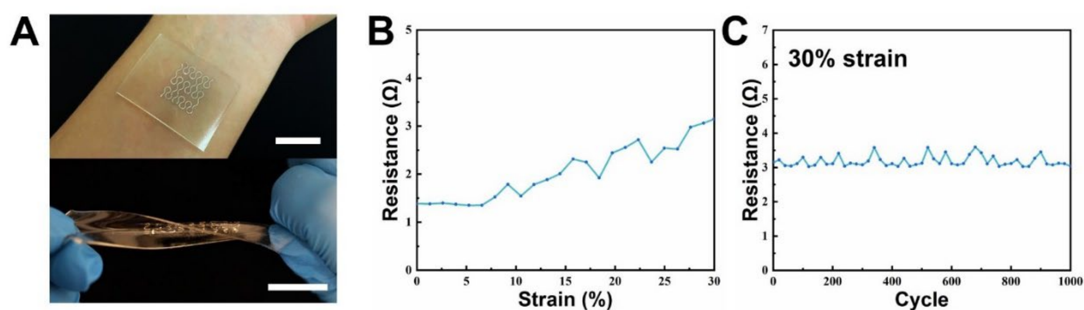

Figure S18. Stretchable horseshoe pattern transferred to PDMS by PVA binder. (**A**) Up: Photo of the Ag horseshoe pattern on PDMS attached to human hand. Bottom: Photo of the Ag horseshoe pattern on PDMS under stretching and twisting state. Scale bar: 2 cm. (**B**) The resistance under 30% strain. (**C**) The resistance during 1000 cycles under 30% strain.

Table S1. The electrodeposition solution and parameters of eight target materials fabricated by ERT method.

Deposited material	Electrodeposition solution	Working electrode
Cu	Commercial Cu plating solution (Caswell, USA), mainly $CuSO_4$	Cathode
Au	Commercial Au plating solution (Caswell, USA)	Cathode
Ni	Commercial Ni plating solution (Caswell, USA), mainly $NiSO_4$	Cathode
Zn	Commercial Zn plating solution (Caswell, USA), mainly $ZnCl_2$	Cathode
CdS [1]	$Cd(NO_3)_2$, 0.05 M, $Na_2S_2O_3$, 0.025 M pH~2 (HCl)	Cathode
MnO_2 [2]	$Mn(CH_3COO)_2$, 0.01 M Na_2SO_4, 0.02 M	Anode
PPy [3]	Pyrrole, 0.1 M KNO_3, 0.3 M	Anode
PANi [4]	Aniline, 0.5 M H_2SO_4, 1 M	Anode

The main components in the Caswell plating solutions were referred to the corresponding material safety data sheet (MSDS). The specific names and components in Au plating solution have been withheld as a trade secret. (https://www.caswellcanada.ca/MSDS.html)

Table S2. The resistivities (ρ) of materials involved in the templates used in ERT process.

	Au	Cr	Cr_2O_3	Si	SiO_2
ρ (Ω·m)	2.4×10^{-8}	13×10^{-8}	3×10^{4}	10^{-3}-10^{1}	10^{12}-10^{14}

Table S3. The thicknesses (*t*) and sheet resistances (R_s) of different material layers involved in the templates used in ERT process.

	Au/Cr/Si	Cr/Si	Si	Au/Cr/SiO_2	Cr/SiO_2	SiO_2
t (nm)	25/5/(5×10^5)	5/(5×10^5)	5×10^5	25/5/300	5/300	300
R_s (Ω/sq)	0.94	441	74227	1.33	803	∞

As shown in Table S2, the resistivity (ρ) of Cr is 13 × 10^{-8}. The sheet resistance (R_s) of pure Cr film with 5-nm thickness is ~26 Ω/sq. However, the R_s measurements of Cr layer on SiO_2 in our experiment is 803 Ω/sq, which indicates the native oxidation of Cr in the air. Si and Cr with oxidation layer show semiconducting property. As shown in Table S3, the sheet resistances (R_s) of these semiconducting layers show at least two-order higher than that of the conductive Au layer. The R_s difference between the semiconducting substrate and the conductive Au layer can ensure the success of selective electrodeposition under optimized current densities (1.0-2.0 mA/cm^2). As the control group, we checked the Au-patterned template based on non-conductive SiO_2 substrate, which is failed in electrochemical replication of arbitrary pattern (Figure S9).

Table S4. The surface roughness data characterized by AFM of the nano grating template before and after 50 times of fabrication process.

	R_{pv} (nm)	R_q (nm)	R_a (nm)	R_z (nm)	R_{sk} (nm)	R_{ku} (nm)
Original Template	11.259	1.616	1.283	10.468	0.031	2.973
After 50 times of replication	10.573	1.571	1.255	9.942	0.092	2.896

$\mathbf{R_{pv}}$: Peak-to-valley roughness; $\mathbf{R_q}$: Root mean square roughness; $\mathbf{R_a}$: Average roughness; $\mathbf{R_z}$: Maximum height of profile; $\mathbf{R_{sk}}$: Skewness; $\mathbf{R_{ku}}$: Kurtosis.

Table S5. Comparison of ERT with typical patterning techniques in terms of resolution, throughput, and capital cost of equipment.

Patterning technique	Resolution (μm)	Throughput (m^2/h)	Capital cost of equipment ($)
Photolithography	0.007-10	10^{-2}-1	1M-100M
E-beam lithography (EBL)	0.005-0.1	10^{-6}-10^{-3}	1M-5M
Nanoimprint lithography (NIL)	0.01-1	10^{-5}-1	500k-5M
Inkjet printing	20-100	10^{-2}-10	10k-50k
Screen printing	30-100	1-10^{3}	1k-1M
Electrochemical replication and transfer (ERT)	0.05-100	10^{-1}-10^{2}	1k-10k

For these five typical patterning techniques, the data of their resolutions, throughputs and capital costs of equipment were summarized from references [5]. For resolution, it is mainly determined by the smallest feature size. The 7-nm resolution for photolithography and 5-nm for EBL are data obtained from the rigid Si electronics. Direct photolithography on flexible plastic substrates cannot reach such high resolution. Because of charge accumulation on isolating substrate, the resolution of EBL is also limited on flexible substrates. In the flexible electronics, the resolutions based on these patterning techniques are still lower than those on rigid substrates [6]. In 2018, K. Myny proposed the concept of a Moore's law for flexible electronics, with minimum feature size of 200 nm [7]. For throughput, it is generally accepted that the high-volume-production techniques show throughput of more than 100 wafers per hour (WPH, 36 s for 1 wafer) corresponding to >1 m^2/h [8]. In photolithography, only the bottleneck step, i.e., UV exposure step, is taken in account for calculation of its throughput. For ERT process, the bottleneck step is electrodeposition. To calculate its throughput, 1-2 min can finish 1 wafer (30-60 WPH) in 1 electrodeposition bath. Since the equipment cost and power consumption (mA scale current and 0.5-5 V voltage) are ultralow in ERT process, the practical production line can consist of 10-100 or even more parallel electrodeposition baths. A conservative estimate of maximum throughput of ERT can reach 10^2 m^2/h. The capital equipment of ERT process is the ordinary direct current (DC) power supply. In our experiment, we carried out electrodeposition on a source meter (Keithley 2400, Tektronix, Inc., USA), with cost of ~3k $. In practical production, the cost of the DC power equipment can be much lower.

Table S6. Comparison of as-made metal meshes with other typical transparent electrode materials in terms of sheet resistance, transmittance, and figure of merit.

Transparent electrode	Electrodeposition time (min)	Sheet resistance (R_s) (Ω/sq)	Transmittance (550 nm, T) (%)	Figure of merit (FoM)
Cu mesh, ERT	5	26.19	97.1	490
	10	13.52	97.0	900
	15	2.79	96.8	4139
	20	1.33	95.1	5640
	30	0.77	93.5	7163
	40	0.30	87.4	9042
	60	0.18	85.1	12586
	80	0.11	85.0	20254
	100	0.055	77.7	25650
Au mesh, ERT	20	0.64	85.6	3625
Ni mesh, ERT	20	1.86	85.6	1242
ITO film [9]		10	90	348
Graphene [10]		125	97.4	114
CNT network [11]		100	10	35
PETDOT:PSS (Clevios™ PH 1000) [12]		25	85	89
Ag mesh [13]		58	98	320
AgNW network [14]		5	90	697
Ag ultrathin film [15]		9	80	177

The calculation of figure of merit (FoM) is based on the values of sheet resistance (R_s) and transmittance (T) at 550-nm wavelength and follows the equation [16]:

$$FoM = \frac{188.5}{R_s(\frac{1}{\sqrt{T}}-1)}$$

Reference

[1] G. Sasikala, R. Dhanasekaran, C. Subramanian, *Thin Solid Films* **1997**, 302, 71.
[2] S. Chou, F. Cheng, J. Chen, *J. Power Sources* **2006**, 162, 727.
[3] H. Wei, Y. Wang, J. Guo, X. Yan, R. O'Connor, X. Zhang, N. Z. Shen, B. L. Weeks, X. Huang, S. Wei, *ChemElectroChem* **2015**, 2, 119.
[4] Y. Zhong, Z. S. Chai, Z. M. Liang, P. Sun, W. G. Xie, C. X. Zhao, W. J. Mai, *Acs Appl. Mater. Interfaces* **2017**, 9, 34085.
[5] a) K. Fukuda, T. Someya, *Adv. Mater.* **2017**, 29, 1602736; b) A. Pimpin, W. Srituravanich, *Eng. J.* **2012**, 16, 37; c) S. Kim, H. Sojoudi, H. Zhao, D. Mariappan, G. H. McKinley, K. K. Gleason, A. J. Hart, *Sci. Adv.* **2016**, 2, e1601660; d)W. Wu, *Nanoscale* **2017**, 9, 7342; e) D. S. Engstrom, B. Porter, M. Pacios, H. Bhaskaran, *J. Mater. Res.* **2014**, 29, 1792; f) J. Haaheim, O. Nafday, T. Levesque, J. Fragala, R. Shile, presented at *Microfluidics, BioMEMS, and Medical Microsystems VII*, **2009**; g) A. Pirati, J. van Schoot, K. Troost, R. van Ballegoij, P. Krabbendam, J. Stoeldraijer, E. Loopstra, J. Benschop, J. Finders, H. Meiling, presented at *Extreme Ultraviolet (EUV) Lithography VIII*, **2017**; h) G. D. Hutcheson, presented at *Extreme Ultraviolet (EUV) Lithography IX*, **2018**; i) D. M. Tennant, in *Nanotechnology*, Ed: G. Timp, Springer, New York, NY, USA **1999**, Cp. 4.
[6] a)S. H. Ahn, L. J. Guo, *Adv. Mater.* **2008**, 20, 2044; b) K. Scholten, E. Meng, *Microsyst. Nanoeng.* **2016**, 2, 16053.
[7] K. Myny, *Nat. Electron.* **2018**, 1, 30.
[8] R. Garcia, A. W. Knoll, E. Riedo, *Nat. Nanotechnol.* **2014**, 9, 577.
[9] R. B. H. Tahar, T. Ban, Y. Ohya, Y. Takahashi, *J. Appl. Phys.* **1998**, 83, 2631.
[10] S. Bae, H. Kim, Y. Lee, X. F. Xu, J. S. Park, Y. Zheng, J. Balakrishnan, T. Lei, H. R. Kim, Y. I. Song, Y. J. Kim, K. S. Kim, B. Ozyilmaz, J. H. Ahn, B. H. Hong, S. Iijima, *Nat. Nanotechnol.* **2010**, 5, 574.
[11] F. Mirri, A. W. K. Ma, T. T. Hsu, N. Behabtu, S. L. Eichmann, C. C. Young, D. E. Tsentalovich, M. Pasquali, *ACS Nano* **2012**, 6, 9737.
[12] D. Alemu, H.-Y. Wei, K.-C. Ho, C.-W. Chu, *Energy Environ. Sci.* **2012**, 5, 9662.
[13] J. Schneider, P. Rohner, D. Thureja, M. Schmid, P. Galliker, D. Poulikakos, *Adv. Funct. Mater.* **2016**, 26, 833.
[14] J. H. Park, G. T. Hwang, S. Kim, J. Seo, H. J. Park, K. Yu, T. S. Kim, K. J. Lee, *Adv. Mater.* **2017**, 29, 1603473.
[15] H. Kang, S. Jung, S. Jeong, G. Kim, K. Lee, *Nat. Commun.* **2015**, 6, 6503.
[16] M. G. Dressel, G. Gruner, *Electrodynamics of solids: Optical properties of electrons in matter*, Cambridge University Press, Cambridge, UK, **2002**.